Contract No. R2562B020

Complete Research Report

Bacteria immobilized-carbon: Innovation for water and soil

Head of Project

Associate Professor Dr.Puangrat Kajitvichyanukul

Department

Faculty of Engineering, Naresuan University

August 2019

Contract No. R2562B020

Complete Research Report

Bacteria immobilized-carbon: Innovation for water and soil

Co-Researcher

1. Associate Professor Dr.Puangrat Kajitvichyanukul — Naresuan University
2. Dr.Apichon Watcharenwong — Suranaree University of Technology

Support by

Income Budget of Naresuan University

Fiscal Year 2019

Abstract

In this research, the adsorption mechanism of pesticides including atrazine, 2,4-D, dichlorvos, and pymetrozine, and biochar acid modification including corn cob, rice husk, bagasse, and coconut fibre were investigated. The four kinds of biochar were synthesised at different pyrolysis temperatures and holding times in oxygen-limited conditions. The biochar were modified by acid to remove minerals and to improve porosity and specific surface area.

The adsorption experiments of all of the biochar with atrazine were performed to determine the best biochar through comparing their adsorption capacities. The best synthesis conditions of biochar using HCl modification and performance in atrazine adsorption were selected for modification with acids (HCl, HF, H_2SO_4, HF-HCl, HF-H_2SO_4, and HCl-H_2SO_4). After modification of the biochar with acids, it became an efficient adsorbent for the performance of atrazine adsorption. The effectiveness of the different acids for biochar modification were compared. The most effective biochar was selected along with the acid mixture.

The characteristics of the optimum biochar were determined including surface morphology (SEM), specific surface area (BET), the functional groups (FT-IR method), the point of zero charge (pH_{pzc}), the surface chemistry of biochar (Boehm titration method), and the hydrophilic property (Contact angle method). The optimum biochar conducted the adsorption with the pesticides including atrazine, 2,4-D, dichlorvos, and pymetrozine. The effect of pH to the adsorption efficiency of atrazine, 2,4-D, and pymetrozine on biochar were investigated.

The results indicated that when the biomass is burned at high temperatures, the yield of biochar was reduced significantly. However, if the holding time was increased, the yields of biochar only decreased a little. When the pyrolysis temperatures were increased, the maximum adsorption capacities of biochar were significantly increased. When the holding times of the pyrolysis process were increased, the maximum adsorption capacities of the biochar were negligibly increased. However, at high pyrolysis temperatures and the long holding time, the biochar pores were destroyed, consequently leading to the decreasing of the maximum adsorption capacity.

The best of four kinds of biochar were synthesised under different pyrolysis conditions and HCl modification, had the highest atrazine adsorption including CCB600 ^{0}C-4 h, RHB500 ^{0}C-6 h, BAB600 ^{0}C-6 h, CFB600 ^{0}C-4 h. The best of the four kinds of biochar that performed different acid modification which have the highest of atrazine adsorption including: CCB600 ^{0}C-4 h with HF modification (CCB), RHB500 ^{0}C-6 h with HF modification (RHB), BAB600 ^{0}C-6 h with HF-H_2SO_4 modification (BAB), CFB600 ^{0}C-4 h with HCl modification (CFB).

The pHpzc values of the four kinds of biochar CCB, RHB, BAB, and CFB were 0.7 to 0.75. The specific surface area of the four kinds of biochar CCB, RHB, BAB, and CFB were 292.92, 153.27, 67.42, 402.43 m^2/g, respectively. The main distribution in porosity of the four kinds of biochar were micropores (<2 nm) and narrow mesopores (2-20 nm). The functional groups on the biochar surface are an important site for the efficient removal of the pesticides. The four kinds of biochar were tested by the contact angle method which showed hydrophilic properties.

The adsorption capacity depended on the specific surface area and the total pore volume of the biochar. The kinetic models of the pesticides and the four kinds of biochar were fitted into following the pseudo-second-order model. The isotherm model fitted to the Langmuir isotherm which presents the adsorption monolayer of pesticides on the surface of the four kinds of

biochar. However, the adsorption data of the CCB and diclorvos, the RHB and 2,4-D, and the CFB and atrazine fitted the Freundlich model, this shows that the multilayers and heterogeneous adsorption occurred on the surface of the biochars. The isotherm shape of the CFB and pesticides, and the four kinds of the biochar and dichlorvos illustrated the H shape, which are shown to have very strong adsorption capacities. The diffusion model confirmed that the liquid film diffusion was the rate limiting step and the major diffusion mechanism of pesticides onto biochar. The adsorption mechanisms between the four kinds of biochar and pesticides include the pore-filling mechanism and the chemical interaction. However, the chemisorption mechanism between each of pesticides and biochar were different. The H-bonding, hydrophobic bonding, and π–π EDA are interactions in the adsorption mechanism of atrazine, pymetrozine and the four kinds of biochar. H-bonding and π-π EDA interactions participated in the adsorption mechanism of biochar and 2,4-D. For dichlorvos insecticide, H-bonding and hydrophobic interactions were the adsorption mechanism that formed by the functional group structure of dichlorvos and the functional groups of biochar. In the adsorption mechanism of the four kinds of biochar and the four types of pesticide, H-bonding interaction plays an important role and is a main chemical adsorption.

Based on the overall results of this study, biochar including corn cob, rice husk, bagasse and coconut fibre all were highly efficient in pesticide removal. The coconut fibre biochar was shown to be the most effective. Hence, the four kinds of the biochar are useful materials for the removal of environmental pollutants.

บทคัดย่อ

งานวิจัยนี้ เป็นการสังเคราะห์ถ่านชีวภาพและศึกษากลไกลการดูดซับของถ่านชีวภาพกับสารเคมีทางการเกษตรสี่ชนิดคือ อาทราซีน ไดคลอโรฟีนอกซ์ ไดคลอร์วอส และไพมิโทรซีน ในการผลิตถ่านชีวภาพจะใช้วัสดุจากการเกษตรสี่ชนิด ได้แก่ ซังข้าวโพด ข้าวเปลือก ชานอ้อย และใยมะพร้าว โดยใช้กระบวนการไพโรไลซิสในอุณหภูมิที่ต่างกันในสภาวะที่มีออกซิเจนจำกัด และใช้กรดในการสังเคราะห์ถ่านชีวภาพ เพื่อช่วยในการกำจัดแร่ธาตุ ปรับปรุงรูพรุน และพื้นผิวจำเพาะของถ่านชีวภาพ อีกทั้งยังเปรียบเทียบประสิทธิภาพในการดูดซับของถ่านชีวภาพที่ผลิตได้ในสภาวะต่างๆเพื่อให้ได้ถ่านชีวภาพที่มีประสิทธิภาพที่ดีในการดูซับสารเคมีจากการเกษตร

จากการศึกษาหาความสามารถในการดูดซับสารเคมีของถ่านชีวภาพโดยเปรียบเทียบความสามารถในการดูดซับของถ่านแต่ละชนิดพบว่า ถ่านชีวภาพที่สังเคราะห์ได้จากการใช้กรดไฮโดรคลอริก มีประสิทธิภาพในการดูดซับสาร อาทราซีน ได้ดีที่สุด จากการเปลี่ยนแปลงลักษณะพื้นผิวและรูพรุนของถ่านชีวภาพด้วยกรดสามชนิดคือ กรดไฮโดรคลอริก (HCl) กรดไฮโดรฟลูออริก (HF) และกรดซัลฟิวริก (H_2SO_4) ถ่านชีวภาพที่สังเคราะห์ได้จะนำมาศึกษา ลักษณะพื้นผิวและโครงสร้าง(SEM) พื้นที่ผิวจำเพาะ(BET) วิเคราะห์จำแนกประเภทของสาร(FT-IR) การหาประจุที่ผิวเป็นศูนย์(pHpzc) การหาฟังก์ชันบนพื้นที่ผิวโดยใช้การไตรเตรตของโบห์ม(Boehm titration method) คุณสมบัติความชอบน้ำ(Contact angle method) และศึกษากลไกลในการดูดซับของถ่านชีวภาพกับสารเคมีทางการเกษตร

จากการศึกษาพบว่าเมื่อเผาชีวมวลที่อุณหภูมิสูง ผลผลิตถ่านชีวภาพที่ได้จากการเผาลดลง เมื่อเพิ่มระยะเวลาในการเผาให้นานมากขึ้น ผลผลิตถ่านชีวภาพที่ได้จากการเผาลดลงเพียงเล็กน้อยเท่านั้น ในกระบวนการไพโรไลซิสเมื่อเพิ่มอุณหภูมิในการเผา ความสามารถในการดูดซับของถ่านชีวภาพจะเพิ่มขึ้นและเมื่อเพิ่มระยะเวลาในการเผาในกระบวนการไพโรไลซิส ความสามารถในการดูดซับของถ่านชีวภาพจะเพิ่มขึ้นเล็กน้อย อย่างไรก็ตามการเผาด้วยกระบวนการไพโรไลซิสที่อุณหภูมิสูงๆ ในระยะเวลานานจะทำให้รูพรุนของถ่านชีวภาพถูกทำลายอีกทั้งยังลดความสามารถในการดูดซับของถ่านชีวภาพอีกด้วย

จากการศึกษาพบว่า สภาวะที่เหมาะสมในการสังเคราะห์และเผาถ่านชีวภาพแต่ละชนิดคือ การสังเคราะห์ถ่านจากซังข้าวโพดด้วยกรดไฮโดรฟลูออริก ที่อุณหภูมิ 600 องศาเซลเซียส ระยะเวลา 4 ชั่วโมง(CCB600 ^{0}C-4 h) การสังเคราะห์ถ่านจากข้าวเปลือกด้วยกรดไฮโดรฟลูออริก เผาที่อุณหภูมิ 500 องศาเซลเซียส ระยะเวลา 6 ชั่วโมง (RHB500 ^{0}C-6 h) การสังเคราะห์ถ่านจากชานอ้อยด้วยกรดไฮโดรฟลูออริกผสมกับกรดซัลฟิวริก ที่อุณหภูมิ 600 องศาเซลเซียสระยะเวลา 6 ชั่วโมง(BAB600 ^{0}C-6 h) และการสังเคราะห์ถ่านจากใยมะพร้าวด้วยกรดไฮโดรคลอริกที่อุณหภูมิ 600 องศาเซลเซียส ระยะเวลา 4 ชั่วโมง(CFB600 ^{0}C-4 h) เมื่อทดสอบดูลักษณะถ่านชีวภาพแต่ละชนิดพบว่า ค่าประจุที่ผิว(pHpzc) ของถ่านชีวภาพทั้งสี่ชนิด คือ 0.7 – 0.75 ค่าพื้นที่ผิวจำเพาะของถ่านชีวภาพซังข้าวโพด 292.92 ตารางเมตรต่อกรัม ถ่านชีวภาพข้าวเปลือก 153.27 ตารางเมตรต่อกรัม ถ่านชีวภาพชานอ้อย 67.42 ตารางเมตรต่อกรัม และถ่านชีวภาพใยมะพร้าว 402.43 ตารางเมตรต่อกรัม ค่าความพรุนเฉลี่ยของถ่านชีวภาพทั้งสี่ชนิดอยู่ในระดับไมโคร ที่น้อยกว่า 2 นาโนเมตร มีช่องแคบ 2-20 นาโนเมตร สารฟังก์ชันที่พบในถ่านชีวภาพที่ผลิตได้เป็นกลุ่มที่มีประสิทธิภาพในการกำจัดสารเคมีทางการเกษตร และถ่านชีวภาพทั้งสี่ชนิดมีคุณสมบัติในการดูดน้ำได้ดี

ความสามารถในการดูดซับของถ่านชีวภาพทั้งสี่ชนิดจะขึ้นอยู่กับพื้นที่ผิวจำเพาะและรูพรุน ในการศึกษากลไกลการดูซับของถ่านชีวภาพกับสารเคมีทางการเกษตรจะใช้แบบจำลองแบบ pseudo-second-order model

และ Langmuir isotherm อธิบายกลไกลการดูดซับระหว่างสารเคมี กับถ่านชีวภาพที่บนพื้นผิว ในขณะที่การดูดซับของถ่านชีวภาพซังข้าวโพดกับสารไดคลอร์วอส การดูดซับของถ่านชีวภาพข้าวเปลือกกับสารไดคลอโรฟีนอกซ์ และการดูดซับของถ่านชีวภาพใยมะพร้าวกับสารอาทราซีนเหมาะสมกับแบบจำลอง Freundlich model ซึ่งแสดงให้เห็นถึงกระบวนการดูดซับที่ซับซ้อนและแตกต่างกัน รูปแบบ isotherm ของถ่านชีวภาพใยมะพร้าวกับการดูดซับสารเคมีทางการเกษตร และรูปแบบ isotherm ของถ่านชีวภาพทั้งสี่ชนิดกับสารไดคลอร์วอส มีไฮโดรเจนเกิดขึ้น(H) ซึ่งแสดงให้เห็นว่าถ่านชีวภาพที่ผลิตได้มีความสามารถในการดูดซับที่ดี และจากการศึกษาแบบจำลองการแพร่ สามารถยืนยันได้ว่าเกิดกลไกลการแพร่กระจายของสารเคมีเข้าสู่ถ่านชีวภาพ จากปฏิกิริยาในกลไกลการดูดซับของถ่านชีวภาพ กับสารอาทราซีน และไพมีโทรซีน พบว่ามี พันธะไฮโดรเจน(H-bonding) ความไม่ชอบน้ำ และคู่อิเลคตรอนในพันธะ TT-TT EDA เกิดขึ้น ในกลไกลการดูดซับของถ่านชีวภาพกับสารไดคลอโรฟีนอกซ์เกิดพันธะไฮโดรเจน และคู่อิเลคตรอนในพันธะ TT-TT EDA สำหรับปฏิกิริยาของถ่านชีวภาพกับสารไดคลอร์วอส เกิดพันธะไฮโรเจนและความไม่ชอบน้ำในปฏิกิริยา ซึ่งเกิดจากการเกิดปฏิกิริยาระหว่างหมู่ฟังก์ชันของถ่านชีวภาพกับสารไดคลอร์วอส จะเห็นได้ว่าในกลไกลการดูดซับของถ่านชีวภาพทั้งสี่ชนิดกับสารเคมีทางการเกษตรทั้งสี่ชนิดนั้นเกิดพันธะไฮโดรเจนที่เป็นตัวหลักในการดูดซับสารเคมี

จากผลการศึกษา พบว่าถ่านชีวภาพที่ผลิตจาก ซังข้าวโพด ข้าวเปลือก ขานอ้อย และใยมะพร้าวมีประสิทธิภาพสูงในการกำจัดสารเคมีทางการเกษตรทั้งสารเคมีกำจัดวัชพืชและสารเคมีกำจัดแมลง ถ่านชีวภาพจากใยมะพร้าวเป็นถ่านชีวภาพที่มีประสิทธิภาพในการดูดซับมากที่สุด ดังนั้นถ่านชีวภาพทั้งสี่ชนิดจึงเป็นผลิตภัณฑ์ที่มีประโยชน์ในการกำจัดสารตกค้างในสิ่งแวดล้อมต่อไป

Abbreviation

2,4-D	2,4-dichlorophenoxy
2,4-D Na	2,4-D sodium salt
AC	Activated carbon
Atz	Atrazine
BET	Brunauer–Emmett–Teller
BC	Biochar
BAB	Bagasse biochar
CCB	Corn cob biochar
CFB	Coconut fibre biochar
DBT	Dibutyl phthalate
DCP	2,4-dichlorophenol
PAH	Polycyclic aromatic hydrocarbon
EPA	Environmental Protection Agency
FT-IR	Fourier Transform Infrared Spectroscopy
HCl	Hydrochloric acid
HF	Hydrofluoric acid
H2SO4	Sulfuric acid
Pym	Pymetrozine
IARC	International Agency for Research on Cancer
pHpzc	The point of zero charge
PSO	Pseudo-second-order model
PFO	Pseudo-First-order model
RHB	Rice husk biochar

List of Contents

List of Contents (Cont.)

List of Table

List of Table (Cont.)

List of Figures

List of Figures (Cont.)

Chapter 1
Introduction

1.1 Rationale and background of study

In order to improve the yield of the agricultural production, pesticides are applied widely in the agriculture for protection and controlling in pests, weeds and plant pathogens (Damalas & Eleftherohorinos, 2011). Pesticides played a role in the economic agricultural production, and are used for many types of vegetables, fruit, forage, fibre and oil crops and pesticides enhanced the agricultural industry to be successful in many countries (Hattab & Ghaly, 2012). The pesticide manufacturers are very rigorous in processing pesticides to limit their effect on human health and the environment. However, pesticides continue to pose serious risks to human health and the environment. The pervasive use of pesticides pose a threat to human health in two ways: eating contaminated food and drinking contaminated water. Pesticides persist in the soil, water, and air environment from leaching, runoff and spray drift. It effects wildlife, fish, plants and other organisms (Damalas & Eleftherohorinos, 2011).

Atrazine (6-chloro-N2-ethyl-N4-isopropyl-1,3,5-triazine-2,4-diamine) is a herbicide of triazine family. It was used in agriculture to control grass and broad – leaf weeds. Atrazine was applied to some fruit trees such as bananas, citrus groves, coffee, and sugar cane. It was also used for airfields, parking lots and industrial zones (IARC, 1999). Atrazine is highly toxic and has serious effects on aquatic organisms, plants, and people (N. Liu, Charrua, Weng, Yuan, & Ding, 2015).

2,4-D (2,4-Dichlorophenoxyacetic acid) was used in agriculture as an herbicide. It was applied to prevent weeds growing among plantation crops such as sugarcane, oil palm, cocoa, and rubber. Because it is cheap, it was used widely (Trivedi, Kharkar, & Mandavgane, 2016). People and animals absorbed the poison of 2,4-D in many ways including contaminated air, drinking water, soil and in food. Farmers working in the agriculture sector and workers in the factory to produce 2,4-D are all at risk from the poison (Qurratu & Reehan, 2016).

Dichlorvos is an organophosphate insecticide, it was used to control flies, mosquitoes, ticks, cockroaches, clover mites, crickets, cutworms, grasshoppers, and sod webworms (EPA, 2006b). Dichlorvos was used in domestic, agricultural and veterinary fields (Australian, 2008). Dichlorvos was absorbed very fast in many ways. It has high toxicity in oral and it was classified as more hazardous by WHO (W. H. O. WHO, 2007). Dichlorvos is highly toxic to aquatic invertebrates, honeybees, parasites, predatory species, and earthworms (Australian, 2008).

Pymetrozine is a new insecticide that is highly active against insect pests. It is used widely in the world to control aphids and whiteflies in the field. Pymetrozine was applied to vegetables, cotton, ornamentals, deciduous fruit, and citrus (Degheele, 1998). Pymetrozine had a low acute toxicity to humans, mammals, birds, aquatic organism, and bees. The study of acute toxicology of pymetrozine ranges in toxicity categories III and IV of the technical-grade (E. P. A. EPA, 2000).

Biochar consists of a rich carbon that is obtained through pyrolysis from biomass under oxygen-limited conditions. Biochar has high potential to solve the contaminant efficiently in the water. The biomass for biochar synthesis is readily available and at low cost. Moreover, the large surface area, porous structure, functional groups, and mineral component are special properties of biochar (Saleh, Kamarudin, Ghania, & Kheang, 2016). Washing is a role important for biochar, as the minerals persist on the biochar after the pyrolysis process. The surface of biochar is blocked by minerals and tars, hence, acid-washing treatment is very important to reduce and remove minerals (Y. Zhang, Liu, Chen, & Zheng, 2016).

There are many methods to effectively treat pesticides in waste water, soil, etc. These include thermal treatment (incinerators, open burning), chemical treatment (O3/UV, hydrolysis, Fenton, and photocatalyst), physical treatment (adsorption) and biological treatment (composting, bioaugmentation and phytoremediation) (Hattab & Ghaly, 2012). The adsorption method is a method that is applied widely to remove pesticides, heavy metals, and dyes in water and the soil environment (Narayanan, Gupta, Gajbhiye, & Manjaiah, 2017). The adsorption method is a simple design. The adsorption method incurs lower costs and therefore needs a lower cash outlay (Saleh et al., 2016).

In this study, biochar were prepared from four types of biomass including corn cob, rice husk, bagasse, and coconut fibre. The biochars were synthesised by a slow pyrolysis method under oxygen-limited conditions. The pesticide removals by biochars in the aqueous solution consisted of atrazine, 2,4-D Na, dichlorvos, and pymetrozine. In this research, the study consists of five parts:

1. Preparing the biomass materials to synthesise biochars: The biomass was gathered in Northern Thailand including corn cob, rice husk, bagasse, and coconut fibre. The synthesis process was performed in the ceramic crucible and burnt in a furnace under oxygen-limited conditions. The pyrolysis conditions were investigated including different holding times and pyrolysis temperatures.

2. Preparation and characterization of biochars: Biochars were crushed and modified by acids before analysis and the characterization of biochars, including surface morphology (SEM), specific surface areas (BET), the functional groups (FT-IR), the point of zero charge (pHpzc), the surface chemistry (acid and base groups), and hydrophilic properties.

3. The performing of adsorption experiments for four kinds of biochar and atrazine. The comparison of the adsorption capacity of atrazine by different kinds of biochar. The best biochar of the four kinds was selected according to performance and adsorption. The experiments were done with 2,4-D Na, dichlorvos, and pymetrozine.

4. Study the adsorption isotherm (Langmuir and Freundlich isotherms), the adsorption kinetics (pseudo-first-order and pseudo-second-order models), the intraparticle diffusion model, and the diffusion mechanism of four kinds of biochar and the pesticides.

5. Explore the adsorption mechansim between the four kinds of biochar and the four types of pesticide.

1.2 The objectives of the study

Main-objective: To improve the quality of biochar and enhance the ability of biochar for pesticide removal which are explanted by the adsorption isotherm, adsorption kinetic, and the adsorption mechanisms of pesticides and biochar.

Sub-objectives:

1. To synthesise four types of biochar including corn cob, rice husk, bagasse, and coconut fibre at different pyrolysis temperatures and holding times.

2. To modify the four kinds of biochar with acids and mixtures of acids to remove minerals from the surface area of the biochar.

3. To analyse the biochar characteristics including surface morphology, specific surface area and total pore volume, the functional groups, and the point of zero charge (pHpzc), the surface chemistry (acid and base groups), and hydrophilic properties.

4. To perform the adsorption method to remove atrazine from the aqueous solution using the four types of biochar after washing them with acids. Comparisons are made between the atrazine adsorption capacities of the different types of biochar and to select the best of the four types of biochar which is the highest adsorption capacity.

5. To observe the adsorption process of the best biochar of pesticides including 2,4-D Na, dichlorvos, and pymetrozine.

6. To study the effect of the pH of the solution on the adsorption efficiency of the biochars on the different pesticides.

7. To study the adsorption isotherm, adsorption kinetics, the intraparticle diffusion model, and the diffusion mechanism of the biochar and the pesticides.

8. To investigate the adsorption mechanism of the four kinds of biochar and the four types of pesticides.

1.3 Research Hypotheses

Based on the properties of biochar including the specific surface areas, porous structures, and functional groups, the four kinds of biochar were synthesised under oxygen-limited conditions had high specific surface areas, good porous structures, functional groups after the pyrolysis process. Acid washing improved the porosity and specific surface areas of the biochar. All the biochar tend to be very useful materials that have a high potential to contribute to the treatment of environmental pollutants.

1.4 The scope and limitation of the studies

All the experiments of this study were operated on a laboratory scale. The scope of this research is shown below.

1. The biochar were synthesised from biomass including corn cob, rice husk, bagasse, and coconut fibres which were gathered in Northern Thailand.

2. The biochar were burned at different pyrolysis temperatures and holding times in oxygen-limited conditions.

3. After the pyrolysis process, the biochar was crushed and washed with acids and mixtures of acids (HCl, HF, H2SO4, HCl-HF, HCl-H2SO4, and HF-H2SO4).

4. The characterization of the biochar: The surface morphology of the biochar was analysed by SEM (Scanning Electron Microscope), the specific surface area was measured by BET (Brunauer–Emmett–Teller). The functional groups of the biochar were analysed by FT-IR (Fourier transform infrared spectroscopy) at the Science lab, Naresuan University. The point of zero charge of the biochar were conducted by batch methods, the acid and base groups of the biochar surface were performed according to the Boehm Titration method, and the hydrophilic property was measured with the contact angle method.

5. The adsorption isotherm, adsorption kinetics, the intraparticle diffusion model, and the diffusion mechanism of biochar and the pesticides were studied.

6. The adsorption mechanism of the four kinds of biochar and four types of pesticide were investigated.

7. The pesticides used in the study include atrazine, 2,4-D Na, dichlorvos, and pymetrozine.

Chapter 2
Theoretical background and literature review

2.1 Fundamental knowledge in the properties and the adsorption mechanism of biochar

2.1.1 Properties of biochar

Biochar is a stable solid that is rich in carbon. Biochar is made from biomass such as wood and animal manure. They are used in the soil and also for agricultural gains and carbon sequestration. Biochar that contains carbon can slow carbon emissions to the atmosphere and the degrading of carbon in the form of charcoal (carbon negative). Biochar can be dug into the soil, thereby maintaining carbon levels in the soil and creating the benefit of nutrient rich soil. There are many specific properties that biochar have, such as high surface area, porous structures, functional groups, and mineral components. The advantage of these properties is that they help to enhance the adsorption of pollutants, thus removing them from aqueous solutions. The process of manufacturing biochar requires less energy than the production of activated carbon. It is therefore cheaper to produce biochar than to produce activated carbon. Biochar has new potential as an effective adsorbent including lower price. Feedstocks that are used to produce biochar are readily available at low-cost. Feedstocks come from agricultural biomass and solid waste (X. Tan et al., 2015). The use of invasive plant species to synthesise biochar brought about the reduction of invasive plant species, something that can be useful in protecting the environment (X. Tan et al., 2015).

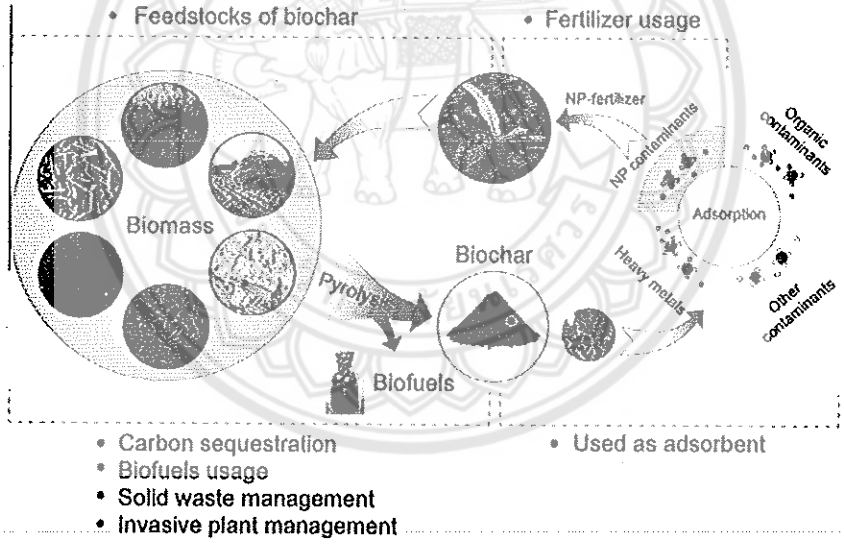

Figure 2.1 The benefits of biochar applied as an effective adsorbent for wastewater treatment
Source: (X. Tan et al., 2015)

Biochar is a renewable resource that is beneficial to the economy and the environment. Biochar is used in environmental technology for water treatment. Many research studies have reported that biochar removed contaminants such as heavy metals, and the pollutants from the soil and water (Figure 2.1). The adsorbent properties of biochar are greater and therefore more effective than activated carbon (X. Tan et al., 2015).

According to Tan et al., biochar adsorbs organic pollutants by means of various interactions. The adsorption mechanism between biochar and organic pollutants consists of electrostatic interaction, hydrophobic effect, hydrogen bonding interaction and a pore-filling

mechanism (2015). The adsorption mechanisms that biochar uses to adsorb organic pollutants is proposed in Figure 2.2

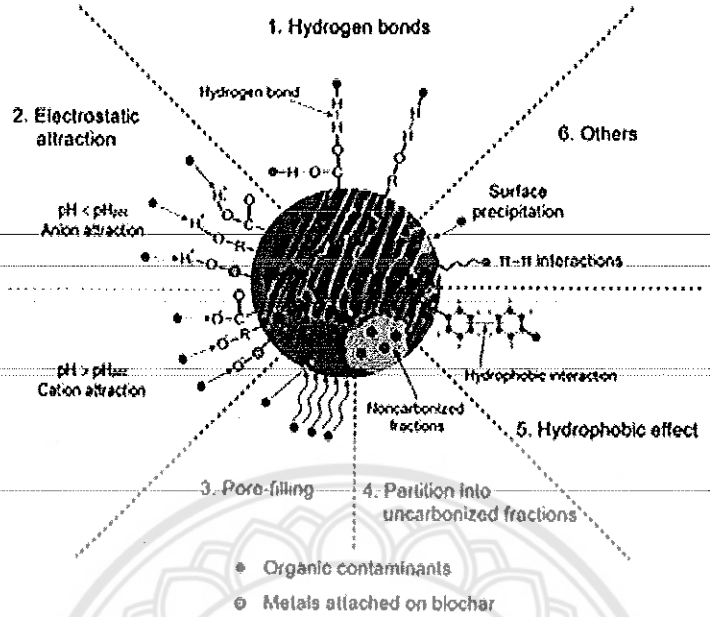

Figure 2.2 The adsorption mechanisms of organic pollutants adsorbed by biochar
Source: (X. Tan et al., 2015)

2.1.2 The adsorption mechanism of biochar

Pore-filling

The porous carbon of biochar is divided into three types, micropores < 2nm, mesopores 2 -50 nm and macropores > 50 nm. However, micropores and small mesopores (2-20 nm) are proposed to present the majority on the surface of biochar. The mechanism of pore-filling on biochar occurs when the pore-filling is in low solute concentrations. Depend on the form of biochar, both polar and non–polar that pore-filling of biochar can adsorb organic pollutants (Inyang & Dickenson, 2015).

Diffusion and partitioning

The organic compounds were diffused in biochar many ways: adsorbates diffuse into pores or into the organic matter of biochar that is, non-carbonized fraction. The later process is similar partition (absorption) mechanism with high concentrations of the solute or biochar is rich in the volatile matter. Partitioning occurs in biochar with a temperature of $\leq 400\ ^0C$, it may contain small aromatic or aliphatic compounds, for example, pyrroles, phenols, ketones, and sugars. Because of the porous nature of biochar, most organic pollutants were adsorbed with some difficultly by biochar. But organic pollutants with hydrophobic molecules are easily adsorbed by partitioning. For instance, atrazine was adsorbed by dairy biochar (200 ^0C) and was adsorbed by swine manure biochar (350 ^0C) (Inyang & Dickenson, 2015).

Hydrophobic interaction

The Hydrophobic interaction mechanism between biochar and organic compounds consists of both partitioning and hydrophobic adsorption. If biochar with low surface oxidation are hydrophobic, they can adsorb hydrophobic organic compounds. For example, Perfluorooctane sulfonate contain the hydrophobic property of a C-F chain, and can adsorb hydrophobic sites on maize straw and willow – derived biochar. Compared with partitioning,

hydrophobic adsorption occurs with low hydration energy on adsorbent surfaces such as between a polar molecule and water molecules (Inyang & Dickenson, 2015).

π-π EDA (electron-donor–acceptor)

π-π EDA is an adsorption mechanism by biochar and the organic compounds. For example, biochar adsorbs atrazine, this link is between chlorine and atrazine and the aromatic carbon on the biochar surface. The link is between the aniline ring in sulfamethoxa – zole (SMX) and π–π electron rich graphene surface of biochar(Inyang & Dickenson, 2015).

Cation-π interaction

Biochar consists many cations such as Fe, Mg, Si, K or Ca which can form interaction with polycyclic aromatic hydrocarbons (PAH) of biochar (Inyang & Dickenson, 2015).

Electrostatic interaction

Electrostatic interaction is a sorption mechanism between the ionic adsorbates and the biochar surface. Cationic organic compounds tend to adsorb negative charges on the surface of the biochar. In contrast, anionic adsorbates tend to adsorb the positive charges on the surface of the biochar. Moreover, pH can affect the adsorption process of biochar and adsorbates, because the surface of the biochar was controlled by the pH of the solution. If the solution pH is lower than the pH of point zero charge (pHpzc) of the biochar, then the surface of the biochar will be positively charged. If the solution pH is higher than the pHpzc of the biochar, the surface of the biochar will be negatively charged (Inyang & Dickenson, 2015).

Hydrogen bonding

The polar organic groups on the surface of the biochar can participate in H-bonding. Many polar groups on biochar facilitate water sorption and impellent H-bonding between biochar and organic pollutants. For example, the rice straw and swine manure biochar can adsorb Dibutyl Phthalate (DBT), this sorption is H-bonding between H–donor group on biochar and O atom on the DBT ester group (Inyang & Dickenson, 2015).

The hydrophilic property

The hydrophilic property of biochar was correlated with the pyrolysis temperature. The biochar synthesised at 300 ^{0}C indicated extremely hydrophobic properties. Whereas, the biochar synthesised from 400 to 600 ^{0}C presented hydrophilic properties (Kinney et al., 2012). The hydrophilic properties of biochar allowed water to enter the pores of biochar (Z. Liu, Dugan, Masiello, & Gonnermann, 2017).

2.2 Synthesis biochar

Thermochemical processes that produce non–activated biochar and activated biochar or carbon, consist of, slow pyrolysis, fast pyrolysis, and gasification. But the production of biochar synthesised from slow pyrolysis, yields more biochar than fast pyrolysis or gasification. The content of biochar from slow pyrolysis, fast pyrolysis, and gasification are 30, 12, and 10 %, respectively. The production of biochar shown in Figure 3 (Inyang & Dickenson, 2015).

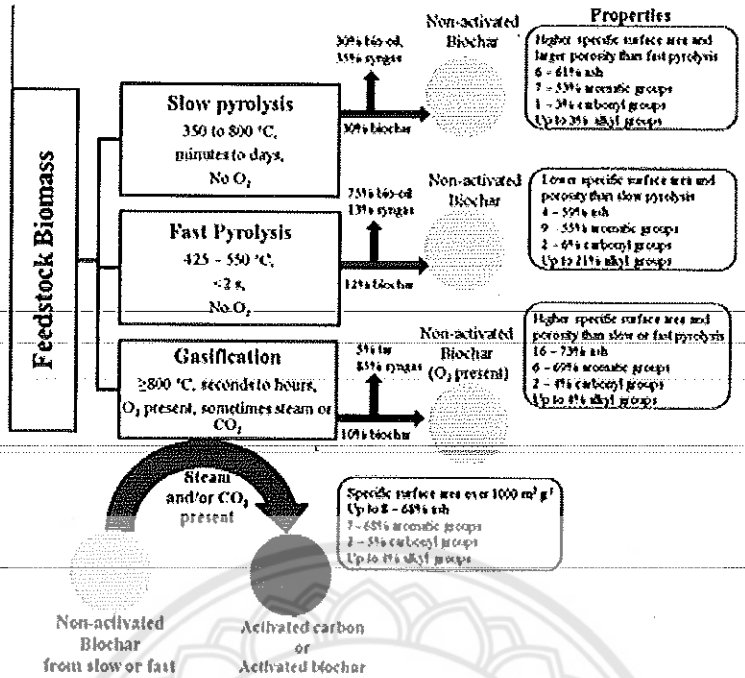

Figure 2.3 The products, yields and characteristics of biochar as synthesised under different pyrolysis conditions
Source: (Inyang & Dickenson, 2015)

Biochar was produced from slow pyrolysis at temperature 350 - 800 ^{0}C and holding times of pyrolysis were from minutes to days. If the pyrolysis temperatures and holding times are increased, the surface area and pore volumes of biochar will increase. For instance, the surface area of oak biochar is from 2 to 225 m^2/g when the temperature is increased from 450 to 650 ^{0}C at 3 hours. The surface area of pig manure biochar is from 23 to 32 m^2/g, when the temperature is increased from 350 to 700 ^{0}C at 2 hours.

Biochar from slow pyrolysis below 600 ^{0}C did not change the chemistry of their parent feedstock, but where the temperature is above 600 ^{0}C, aliphatic groups will change, for example, phenols and carboxylic acids can convert to neutral or fused basic aromatic groups. The pig manure biochar was produced at 620 ^{0}C for 2 hours, the NCH and N-C=O group were not found in the raw manure. The polycyclic aromatic compounds that were formed include such as dioxins and furans in slow pyrolysis at 350-500 ^{0}C and holding time was less than 1 hour (Inyang & Dickenson, 2015).

2.2.1 The conditions effect to characteristics of biochar

The original biomass effects of the adsorption of biochar

Biomass contains compounds including cellulose, hemicellulose and lignin and these compounds converted to biochar carbon matrix. The compound converted to biochar at different temperature ranges. For instance, hemicellulose degraded in a range from 200 to 260 ^{0}C. Cellulose degradation occurred in a range from 240 to 350 ^{0}C. And lignin degradation occurred in a range from 280 to 500 ^{0}C. On the other hand, the original biomass has the amount of minerals that can affect biochar properties, the minerals were ash content after the burning process (Yavari, Malakahmad, & Sapari, 2015). The ash can cap the pores of the biochar leading to a decrease in a specific surface area and the sorption of biochar. So, it is very important to remove ash from biochar when biochar is used in adsorption. In order to decrease the amount of ash, the biomass could be washed with acid after pyrolysis (Uchimiya, Wartelle,

& Boddu, 2012). In contrast, some research reported that high amounts of minerals in the biochar are more able to enhance the sorption capacity of the biochar (Yavari et al., 2015).

The components of biochar depended on the biomass. For instance, wood has a high percentage of lignin, aromatic organic composition, high surface area and low ash content. Herbaceous plants contain high amounts of silica, while animal manures contain more ash (Yavari et al., 2015).

The size of the biomass affects the ash composition of biochar. One study reported that the different sizes of bagasse were in the range of 0.25 to 4.75 mm and was pyrolysed in pure nitrogen gas. It showed that the sizes of bagasse were from 0.25 to 0.6 mm is a large amount of ash in the biochar (Yavari et al., 2015).

The temperature synthesis process effects the specific surface area

Many studies reported that different pyrolysis temperatures impacted on the sorption of organic molecules onto biochar. The non-carbonized domain of biomass converts to a carbonized domain depending on the pyrolysis temperature. The pyrolysis temperature is also affects the specific surface area of the biochar. For example, the synthesis of pine needle derived biochar, the temperature rises from 100 to 700 ^{0}C and the surface area was from 0.6 – 490.8 m^2/g. Wood chips were pyrolysed at temperatures from 450 to 850 ^{0}C in a furnace. At such high temperatures, the biochar develops a high specific surface area (566 m^2/g) and a strong affinity with fungicides. At low temperatures, the biochar has a low surface area (27 m^2/g). The biochar adsorbs pesticides via two mechanisms, viz. the adsorption on the surface area and micro–pores of biochar.

The ash content in the biochar was also correlative with the pyrolysis temperature. The ash content of pine needles was from 1.05 to 2.20 % when the pyrolysis temperature rose from 100 to 700 ^{0}C. The ash content of pig manure biochar rose from 35.7 % to 69.6 %, when the pyrolysis temperature increased. At lower temperatures (200 ^{0}C), the biochar exhibited more affinity for sorption, because there are high amounts of organic carbon and the polymer aliphatic fraction (Yavari et al., 2015).

According to Inyang and Dickenson, if biochar is synthesised at temperatures lower than 600 ^{0}C, it may retain its biomass chemistry. But when the temperature is increased to higher than 600 ^{0}C, some functional groups are converted. For example, aliphatic group converted to neutral or fused basic aromatic groups. The pig manure biochar performed at 620 ^{0}C for 2 hours, it did not retained the NCH and N-C=O groups originally, but the most of aromatic or olefinic –C=C– group were converted and retained in the biochar.

Thermogravimetric analysis of biochar

Biomass consists of the main components including cellulose, hemicellulose, and lignin. Because of the molecular structure, hemicellulose has a short molecular structure with many branches, so they need high thermal activity to
decompose. Conversely, cellulose is more stable in thermal conditions than hemicellulose. Cellulose has a highly linear and non-branching polymer. Lignin is rich in aromatic rings and has a strong cross-linked lead which makes it difficult to decompose. There is a large thermal range in the decomposition temperature of hemicellulose, cellulose and lignin are 200 - 380 ^{0}C, 250 - 380 ^{0}C, and 180 - 900 ^{0}C, respectively (D. Chen, Zhou, & Zhang, 2014).

The heating rate, gas pressure, flow rate, and reaction residence time effect to the adsorption of biochar

The next parameters to determine the characteristics of biochar are the heating rate, and gas pressure, flow rate, and reaction holding time. Cetin et al., 2004 experimented with radiata pine, spotted gum, and bagasse. When the low heating rate was 20 ^{0}C per second, the biochar

developed microporous structures. A high heating rate was 500 ^{0}C per second, where plastic deformation occurred in the biochar causing the formation of macropores in the biochar structure. The heating rate has a strong effect on the development of porous structures and the surface area of the biochar. The high pesticide sorption capacity of biochar was studied using different biomasses under slow pyrolysis conditions. The low heating rate is 5 ^{0}C to 30 ^{0}C per minute and a long residence time. The yield of biochar was 15 - 89 % and biochar has microporous (Yavari et al., 2015).

The oil palm stone biochar has a maximum surface area (320 m^2/g) and a good microporous structure when they are synthesised at high temperatures such as 800 ^{0}C with a period of holding time for 3 hours in the furnace. Biochar synthesised at the temperature threshold, can create a high specific surface area. If the pyrolysis temperature is over the temperature threshold of the biochar, it could lead to a decrease of the specific surface area of the biochar. For example, the surface area of the biochar was synthesised at 800 ^{0}C and 900 ^{0}C for 4 hours were 300 m^2/g and 200 m^2/g, respectively. Biochar synthesised at a high temperature results in the structure of biochar melting, fusion, and shrinkage (Guo & Lua, 1998) (Yavari et al., 2015).

2.2.2 Determination of characteristics of biochar

pHpzc of the biochar

The point of zero charge (pHpzc) is the pH value at the equilibrium between the sum of the surface positive charges and the sum of the surface negative charges (Gatabi, Moghaddam, & Ghorbani, 2016). pHpzc is pH at the zero net charge. The batch equilibration method was one method that could be used to determine the pHpzc of biochar powder. This method is based on the assumption of the protons (H^+), and hydroxyl groups (OH^-), these groups are the potential determining ions. H^+ and OH^- were adsorbed by the particles of biochar. The pH of the solution affects the net surface charge of each particle. The dissociation or association of an additional proton in the solution of the surface groups of the biochar, depending on the pH of the solution and the characteristics of the biochar powder. The positively charged surface occurred when the surface reacted the proton of the acid solution, and the negatively charged surface occurred when the surface loss of the protons under basic conditions (Cerovic´ et al., 2007).

Washing biochar after pyrolysis process

Acid washing is important for biochar as the minerals will persist on the biochar after the pyrolysis process and blocked the pores on the surface of the biochar. Acid washing is, therefore, very important to remove and reduce mineral residue. Several methods could be used to wash biochar with acid. Biochar synthesised from a giant reed (Arundo donax) was rinsed with 1 M HCl and 1M:1M HCl-HF solution (Y. Zhang et al., 2016). In order to remove excess ash, biochar was washed by 0.1 M HCl with a ratio of 27 g of biochar per litre of acid for 1 hour (Uchimiya et al., 2012). In one experiment biochar that was washed by 1 M H_2SO_4 was compared with biochar that was washed with DI water. A dosage of 1.5 g of biochar was immersed in 30 ml of water or acid. The biochar were agitated in an ultrasound bath for 2 hours. The result showed that the pores of biochar treated by H_2SO_4 was cleaner and the pores were clearer than in biochar that was treated using only H_2O (Gai et al., 2014).

The chemical surface (acid and base groups) of the biochar

The acid groups consist of carboxyl, lactonic and phenolic, while, the base groups include ketone. The acid and base groups play an important role in enhancing the efficiency of pollutant removal (Hai Liu et al., 2015).

Chapter 3
Research methodology

3.1 Introduction

The research methodology used in this project is divided into five parts as seen bellow:

The first part was the preparation of the biochar.

The second part was the modification biochar by 0.1 M HCl, analysis the characterization of biochar (SEM), and the adsorption experiments between four kinds of biochar and atrazine.

The third part was the modification of biochar with acids and acid mixtures. The adsorption of atrazine by biochar was performed and observed. An analysis of the characteristics of biochar was carried out.

The fourth part was the adsorption experiments with biochar and pesticides. The adsorption isotherm, the adsorption kinetics, the intraparticle diffusion model, the diffusion mechanism, and the effect of the pH of the solution on the efficiency of pesticide adsorption by the biochar.

The final part was the exploration of the adsorption mechanism of the four types of biochar.

The details of each part are as follow:

3.2 Preparing of the biomass materials and the synthesis of biochar

Objective: To prepare the biomass materials and synthesise the biochar.

The biomasses for biochar synthesis were collected in Northern Thailand including corn cob, rice husk, bagasse, and coconut fibre. Corn cob and bagasse were fresh materials, so they were dried before the synthesis process. In order to remove the moisture that was obtained from the biomass, they were left in the sun for four days. Coconut fibre and rice husk were dry materials, coconut fibre were chopped approximately 1 cm^3 size. All biomasses were dried in the oven at 105 ^{0}C until a constant weight was achieved. After removing the moisture, the biomass were insert into the ceramic crucible and were burned in a furnace (Nabertherm, Germany). The temperature in the furnace was raised slowly at 3 ^{0}C per minute (Krzesin'ska & Zachariasz, 2007). To compare the adsorption capacity of the biochar under various burning condition, the first parameter: the four kinds of biochar were burned over 6 hours and at different pyrolysis temperature - were in the range of 400 to 600 ^{0}C.

The second parameter: the different heating times were in the range of 2 to 6 hours at 600 ^{0}C. All the pyrolysis processes were conducted under oxygen-limited conditions.

In order to estimate the weight loss of biomass and the biochar yield, the mass balances of the biomass were evaluated before and after the burning process. The synthesis processes of the biochar are showed in Figure 3.1

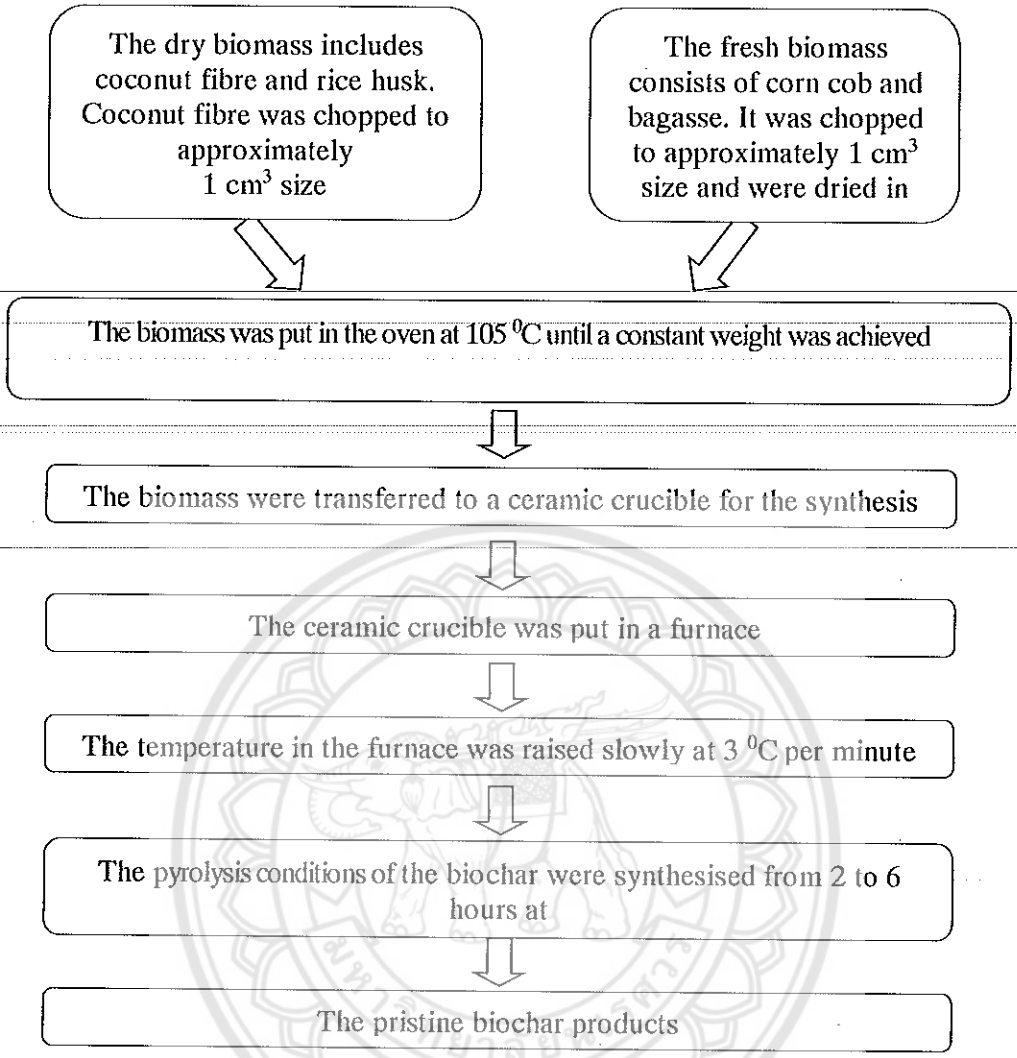

Figure 3.1 Flow diagram of the synthesis biochar method
Source: (N. Liu et al., 2015)

Table 3.1 The pyrolysis conditions of the four kinds of biochar

No	Biomass materials	Pyrolysis temperatures	olding times	Abbreviation of biochar
1	Corn cob	400 ^{0}C	6 hours	CCB400 ^{0}C-6 h
	Coconut fibre			CFB400 ^{0}C-6 h
	Bagasse			BAB400 ^{0}C-6 h
	Rice husk			RHB400 ^{0}C-6 h
2	Corn cob	450 ^{0}C	6 hours	CCB450 ^{0}C-6 h
	Coconut fibre			CFB450 ^{0}C-6 h
	Bagasse			BAB450 ^{0}C-6 h
	Rice husk			RHB450 ^{0}C-6 h
3	Corn cob	500 ^{0}C	6 hours	CCB500 ^{0}C-6 h
	Coconut fibre			CFB500 ^{0}C-6 h
	Bagasse			BAB500 ^{0}C-6 h
	Rice husk			RHB500 ^{0}C-6 h
4	Corn cob	550 ^{0}C	6 hours	CCB550 ^{0}C-6 h
	Coconut fibre			CFB550 ^{0}C-6 h
	Bagasse			BAB550 ^{0}C-6 h
	Rice husk			RHB550 ^{0}C-6 h
5	Corn cob	600 ^{0}C	6 hours	CCB600 ^{0}C-6 h
	Coconut fibre			CFB600 ^{0}C-6 h
	Bagasse			BAB600 ^{0}C-6 h
	Rice husk			RHB600 ^{0}C-6 h
6	Corn cob	600 ^{0}C	2 hours	CCB600 ^{0}C-2 h
	Coconut fibre			CFB600 ^{0}C-2 h
	Bagasse			BAB600 ^{0}C-2 h
	Rice husk			RHB600 ^{0}C-2 h
7	Corn cob	600 ^{0}C	3 hours	CCB600 ^{0}C-3 h
	Coconut fibre			CFB600 ^{0}C-3 h
	Bagasse			BAB600 ^{0}C-3 h
	Rice husk			RHB600 ^{0}C-3 h
8	Corn cob	600 ^{0}C	4 hours	CCB600 ^{0}C-4 h
	Coconut fibre			CFB600 ^{0}C-4 h
	Bagasse			BAB600 ^{0}C-4 h
	Rice husk			RHB600 ^{0}C-4 h
9	Corn cob	600 ^{0}C	5 hours	CCB600 ^{0}C-5 h

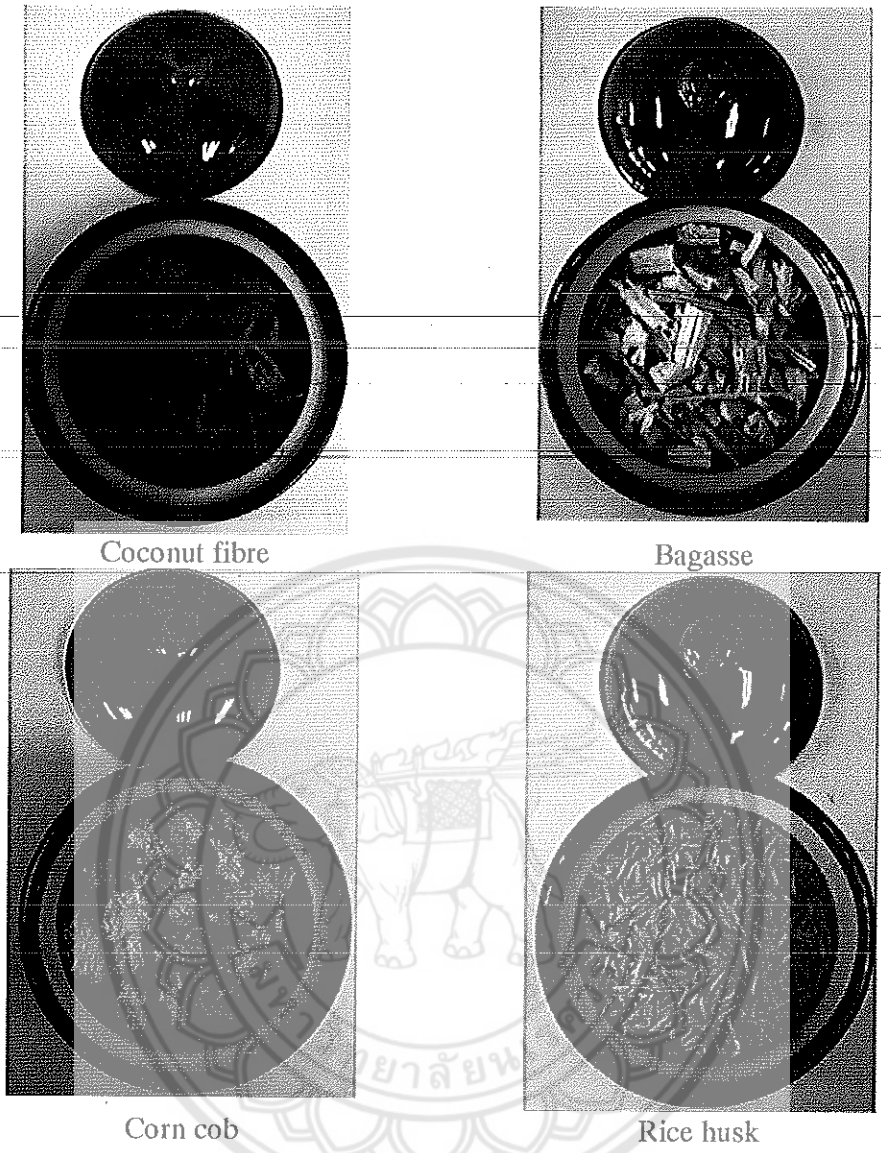

Figure 3.2 The biomass materials in ceramic crucibles

3.3 The modification and characterization of biochar (SEM) and the adsorption experiments between the biochar and atrazine

The modification of biochars by 0.1 M HCl and analysis the morphology of biochar surfaces (SEM)

Objective: To remove the minerals on the surface of the biochar and analyse the surface morphology of biochar.

In order to prepare for the characterization and adsorption experiments of the biochar, they were crushed by pestle and mortar and passed through a 0.8 mm sieve. The biochar was washed with 0.1 M HCl acid to remove excess minerals, the ratio of biochar and 0.1 M HCl acid was 27 gram/L (Uchimiya et al., 2012). Then, the biochar was rinsed with deionized water until the pH of the solutions reached neutral. The biochar was put in the oven at 80 ^{0}C overnight (Uchimiya et al., 2012). The final biochar products were in powder form.

The surface morphology of the biochar was analysed by scanning electron microscope (LEO 1455 VP model, Carl Zeiss Microscopy GmbH, England).

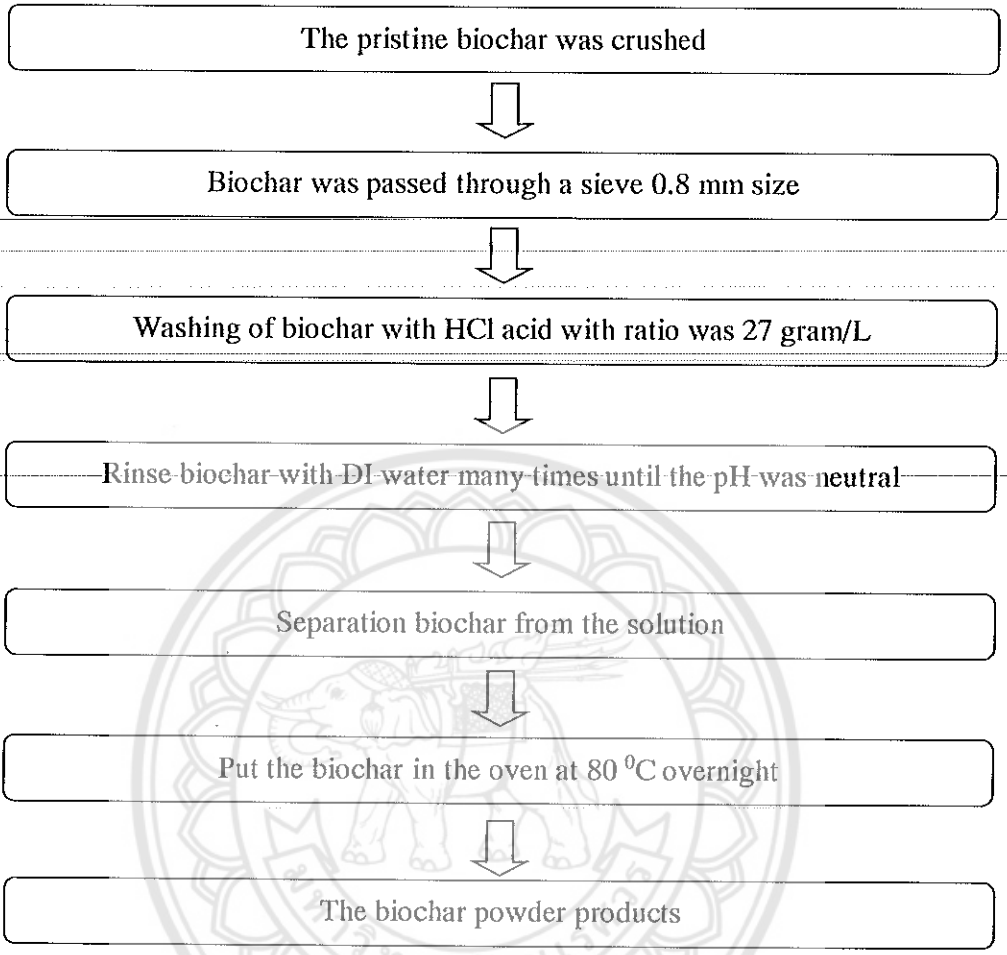

Figure 3.3 Flow diagram of the process of preparation and washing biochar

The experimental performance of the adsorption of atrazine by the different biochars

Objective: To select the best biochar through the high atrazine adsorption capacities of biochar.

The adsorption process of the four kinds of biochar and atrazine were conducted. The comparison of the maximum atrazine adsorption capacities were performed to choose the most effective biochar. The details of the adsorption method are shown in the next section.

3.4 The modification of biochar with acids and acid mixtures, the atrazine adsorption performance as shown experimentally with the selection and analysis of the characteristics of the most effective biochar

The biochar was modified with acids and acid mixtures, and the adsorption experiment was conducted with atrazine

Objective: To compare the high adsorption capacity of biochar that has been modified with acids and the acid mixtures.

The biochar were modified by different acids and acid mixtures (HCl, HF, H_2SO_4, HF-HCl, HF-H_2SO_4, and HCl-H_2SO_4). Then, the modified biochar were tested to assess its atrazine

adsorption performance. The comparison of the atrazine adsorption capacities of modified biochar were conducted to select the best performing biochar. The detail of the adsorption method is shown in the next section.

The characteristics of the four kinds of biochar

Objective: To explore the characteristics of biochar synthesised under oxygen-limited conditions.

Characterization of the biochar using SEM, BET, and FT-IR

The surface morphology of the four types of biochar were analysed by scanning electron microscope (LEO 1455 VP model, Carl Zeiss Microscopy GmbH, England), the biochar samples were loaded on tape coated with gold before analysing. The specific surface area and total pore volume of the biochar were measured by BET (Brunauer–Emmett–Teller) method (TriStar II 3020, Micromeritics Instrument Corporation, USA), the functional groups of biochar were analysed according to the FT-IR method (Frontier, PerkinElmer, Germany). The hydrophilic properties of biochar were determined by the contact angle method (OCA 20, Dataphysics OCA GmbH, Germany).

Determine the point of zero charge of the biochar

According to Liu et al, 2016, the batch experiment was used to determine the pHpzc of biochar, the solution of 0.01 M NaCl was adjusted pH from 2 to 12 using NaOH and HCl. The amounts (0.2 g) of biochar were added to the solutions of 0.01 M NaCl. The final pH was measured after the solution was shaken for 48 hours (N. Liu et al., 2016). The chart of pH_{final} and $pH_{initial}$ was plotted, the pHpzc of the adsorbent was a point of intersection of the "pH_{final} vs $pH_{initial}$" curves (Varsha Srivastava, C. H. Weng, V. K. Singh, & Sharma, 2011).

Determination of acid and base group distribution on the surface of the biochar

To estimate the surface chemistry of biochar, the Boehm titration method was applied to determine the amount of acid, and base groups on its surface. In this experiment, $NaHCO_3$, Na_2CO_3, and NaOH are used to define these acid groups: carboxyl acid; lactone and carboxyl; phenol, lactone, and carboxyl, respectively. HCl was used to determine the base groups (ketonic, pyronic, and chromenic) of biochar. In brief, preparing 50 ml of the solutions of 0.05 M bases ($NaHCO_3$, Na_2CO_3, NaOH) and 0.05 M acid (HCl), then 0.5 g of biochar was added to each of the solutions, and then shaken for 24 hours. After this process, Whatman filter paper 42 was used to separate the filtrate from the solutions. The reactions were completed when 10 ml of HCl and NaOH with a concentration of 0.05 M, were mixed with 1 ml of the filtrates. All these solutions were back-titrated by using 0.05 M of NaOH and HCl. The phenolphthalein is an indicator and was used in this experiment (Mukherjee, Zimmerman, & Harris, 2011), (Chun, Sheng, Chiou, & Xing, 2004). The mathematical formulae were used to estimate the quantity of the surface groups of the biochar as shown below.

$$[HCl]V_{HCl} = [NaOH]V_{NaOH} + \left(\frac{n_{HCl}}{n_B}[B]V_B - n_{CSF}\right)\frac{V_a}{V_B} \quad (1)$$

$$n_{CSF} = \frac{n_{HCl}}{n_B}[B]V_B - ([HCl]V_{HCl} - [NaOH]V_{NaOH})\frac{V_B}{V_a} \quad (2)$$

Where, n_{CSF} (mmol/g) is the mole of surface functionalities of the biochar; n_{HCl}/n_B is the mole ratio of acid to base; [B] (mol/L) and V_B (ml) are the base concentration that were mixed with the biochar; [HCl] (mol/L) and V_{HCl} (ml) are the concentrations and volume of the acid added to the part of base that taken from the original samples; [NaOH] (mol/L) and V_{NaOH} (ml)

are the concentrations and volume that are used in the back – titration; V_a (ml) is the volume that was taken from V_b.
Sources: (Goertzen, The´riault, Oickle, Tarasuk, & Andreas, 2010)

The hydrophilic properties of biochar

The contact angle method was used to determine the hydrophobic and hydrophilic properties of biochar.

3.5 The performance of the adsorption experiments between good biochar and pesticides, the study of the adsorption isotherm, the adsorption kinetics, the effect of pH of solution to the adsorption of biochar and pesticides

The performance of the adsorption experiments between good biochar and pesticides

Objective: To remove the pollutant pesticides by the biochar adsorption and study the adsorption isotherm and the adsorption kinetics of biochar and pesticides.

All the adsorption experiments were performed using the batch adsorption method. The volume of the pesticides and an amount of biochar were added into the Erlenmeyer flasks 250 ml, the dosage of biochar was 1.5 g/L. The Erlenmeyer flasks were shaken (MS Orbital Shaker, MS-NOR-30/MS-NOR-3001) for equilibrium time at 120 rpm in dark conditions. During the adsorption experiment, the pesticide solutions were taken to measure the residual concentrations by UV–Vis spectrometer (Genesys 10S UV-Vis spectrophotometer, Thermo Scientific). The wavelengths of maximum absorbance were found by scanning the absorption spectra of the pesticides. The wavelength to measure the pesticides including atrazine, 2,4-D Na, dichlorvos, and pymetrozine were 229 nm (Ghosh & Philip, 2005), 230 nm, 210 nm (Gomez et al., 2017) (Rahman & Muneer, 2005), and 299 nm (Federal, 2014), respectively. Whatman filter paper 42 with the retention of 2.5 μm was used to separate the biochar from the pesticide solutions. The 5 concentrations of pesticides were prepared to use in adsorption experiments and calculate the adsorption isotherm and adsorption kinetics.

Furthermore, the effect of pH of solutions and the dosage of biochar were explored in the adsorption process. The pH of solution was prepared in the range of 1.0 to 12.0. HCl and NaOH solutions were used to adjust the pH of pesticide solutions. The influencing of biochar dosage on pesticide adsorption was conducted by various biochar dosages which were in the range of 0.25 to 10.00 g per litre of pesticides.

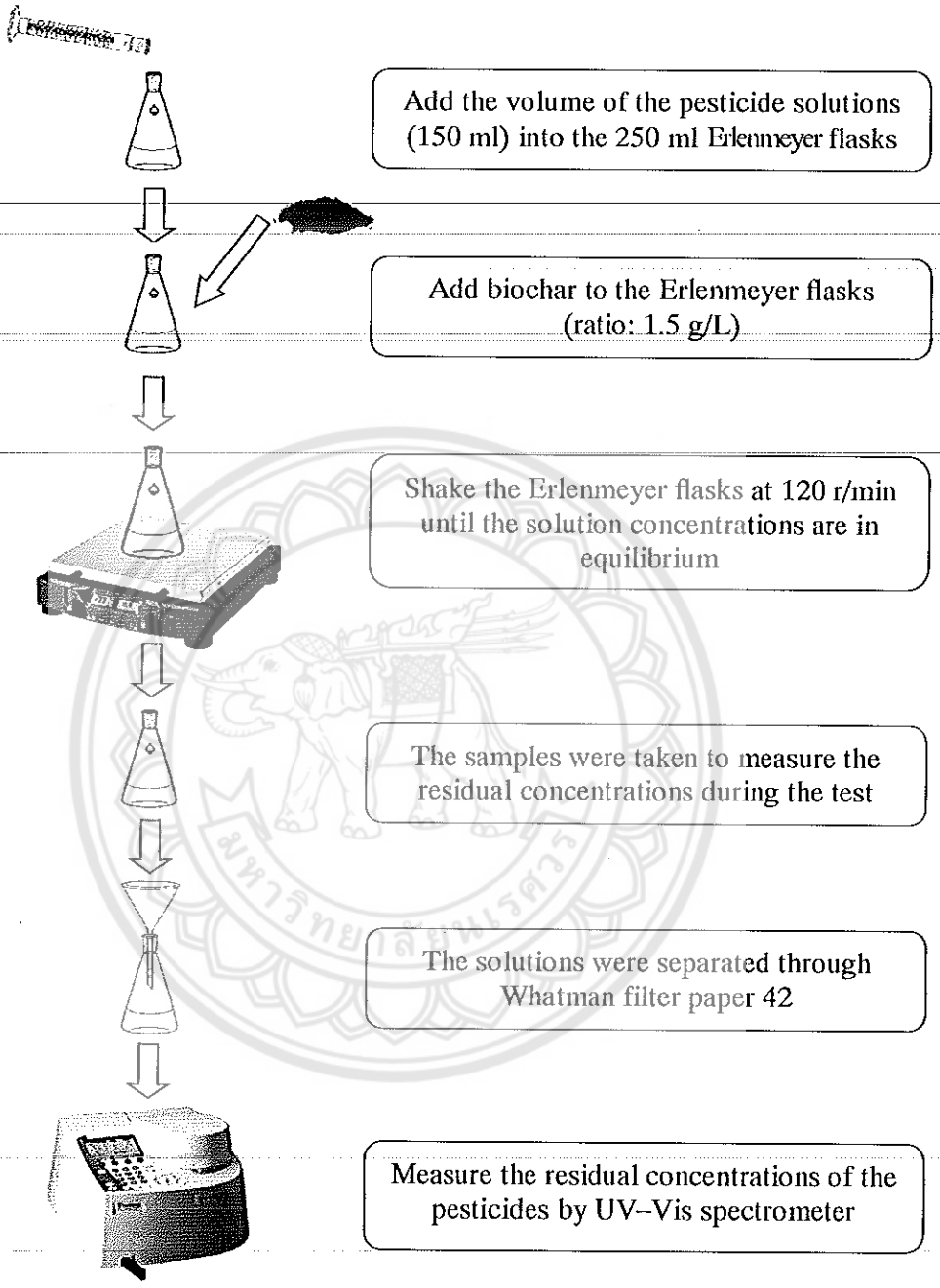

Figure 3.4 Flow diagram of the adsorption experiments of pesticides and biochar
Sources: (N. Liu et al., 2015)

The adsorption isotherms and adsorption kinetics study

Objective: To investigate the parameters of adsorption isotherm and adsorption kinetics.

The adsorption isotherms and adsorption kinetics study of the four kinds of biochar and the pesticides were studied. The investigation of adsorption isotherms includes the Langmuir isotherm and the Freundlich isotherm. The adsorption kinetic models consist of the pseudo-

first-order and pseudo-second-order models, the intraparticle diffusion and the diffusion mechanism were explored.

3.6 The adsorption mechanism of biochar and pesticides

Objective: To explore the adsorption mechanism of biochar and the pesticides.

The adsorption mechanism of the biochar and the pesticides were explored and explained in depth, based on the evidence of the results and theory. The evidence supports the explanation of the adsorption mechanism between the biochar and the pesticides including the SEM, FT-IR analysis, BET method, hydrophilic property, and the acid and base group results of biochar.

Chapter 4
Results and discussion

Chapter 4 presented the results and a discussion of this study. The experimental data are shown below.

4.1 The characterization and the Q_0 of the four kinds of biochar that were synthesised under different pyrolysis conditions

4.1.1 Effect of pyrolysis conditions on the mass loss of the four kinds of biochar

The influence of the pyrolysis temperatures and the holding times to the mass loss of the four kinds of biochar were similar as shown in Table 4.1. Figure 4.1 indicates the mass loss of CCB and a typical graph of biochar that illustrates the effect of pyrolysis temperatures on the mass loss by the pyrolysis process.

In the pyrolysis process, the heating temperature is a factor that has a strong effect on the biochar yield. When increasing the temperature, the mass of the four kinds of biochar decreased. At 100 ^{0}C to 200 ^{0}C, the mass of the biochar slightly decreased from 98.53 % to 82.67 % (Table 4.1). This was likely to be due to the loss of moisture content, this result agrees with previous experimental results (Melo, Coscione, Abreu, Puga, & Camargo, 2013). At 300 ^{0}C, the percentage of the mass of the four kinds of biochar decreased in the range of 42.00 to 53.67 % (Table 4.1), this temperature significantly influenced the loss of biochar. When the temperature was from 400 to 550 ^{0}C, the mass of the biochar decreased from 19.41 to 45.51 % (Table 4.1). The mass of the four kinds of biochar stabilized at a temperature of 600 ^{0}C (Table 4.1). According to Demirbas, biomass consists of cellulose, hemicelluloses, water, lignin, simple sugars, extracts, lipids, proteins, starches, ash, hydrocarbons, and other compounds (Demirbar, 2009). The decreasing of mass is explained through the pyrolysis process, the biomass transformed into biochar, bio-oil, and syngas (Yavari et al., 2015). At high pyrolysis temperatures, the volatile material was transferred and released significantly which changed the yield of the biochar (Guo & Lua, 1998). Therefore, when the biomass is burned at high temperatures, the yield of the biochars were decreased significantly.

The second factor that influenced the decreasing biochar yield was the holding time. When the holding time was increased from 2 to 4 and 6 hours at 600 ^{0}C, the biochar yield percentage decreased slightly (Table 4.1). At a high temperature, high amounts of the volatile matter were released in the initial two hours. The increasing holding time led to the yields that were little decreased (Guo & Lua, 1998).

In summary, the yield of biochar decreased significantly by the high pyrolysis temperature and decreased negligibly by the long holding time at high temperature.

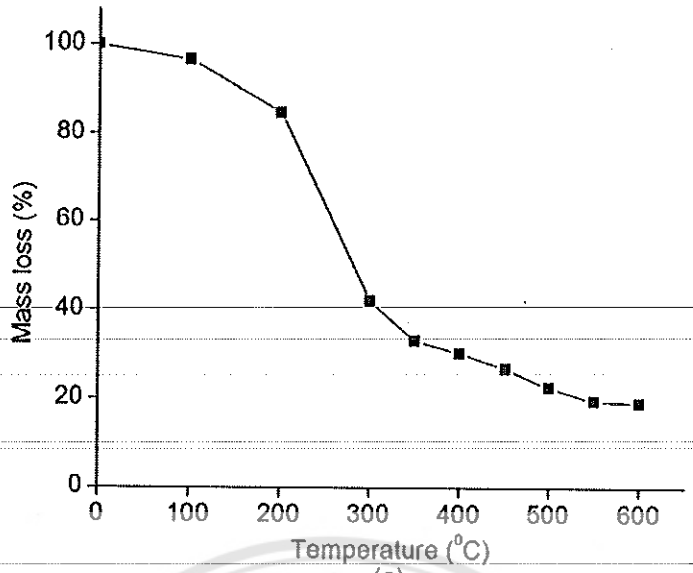

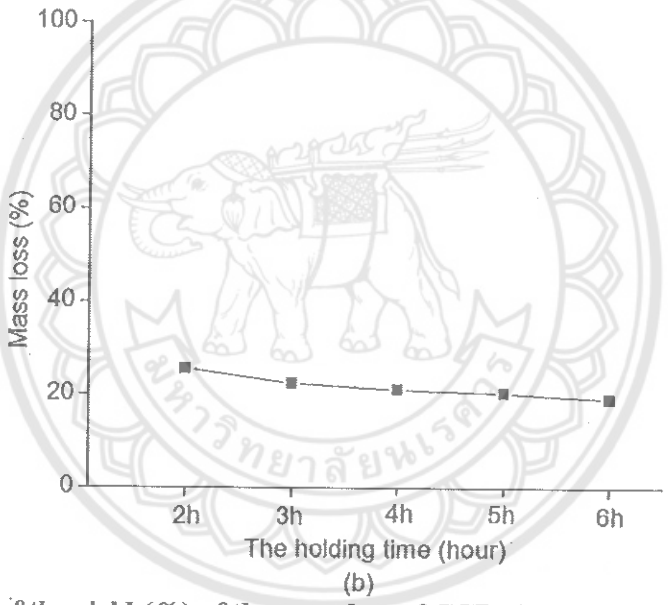

Figure 4.1 Effect of the yield (%) of the mass loss of CCB: (a) the pyrolysis temperatures, (b) the holding times

Table 4.1 The yield (%) of four kinds of biochar effected by pyrolysis temperatures and holding times

Biochar		Corn cob	Rice husk	Bagasse	Coconut fibre
Synthesis for 6 h	100 ^{0}C	96.56	98.53	95.53	97.41
	200 ^{0}C	84.67	86.67	82.67	87.47
	300 ^{0}C	42.00	53.67	42.6	42.94
	400 ^{0}C	30.21	45.51	34.64	32.38
	450 ^{0}C	26.76	42.96	29.62	28.71
	500 ^{0}C	22.44	38.90	26.80	27.79
	550 ^{0}C	19.41	37.68	25.19	24.53
	600 ^{0}C	18.97	34.72	22.33	21.91
Synthesis at 600 ^{0}C	2 h	25.59	38.99	28.17	28.96
	3 h	22.38	37.88	26.93	26.82
	4 h	21.06	36.87	25.47	24.38
	5 h	20.29	35.93	23.50	23.59
	6 h	18.97	34.72	22.33	21.91

Corn cob Rice husk

Figure 4.2 The pristine biochar products

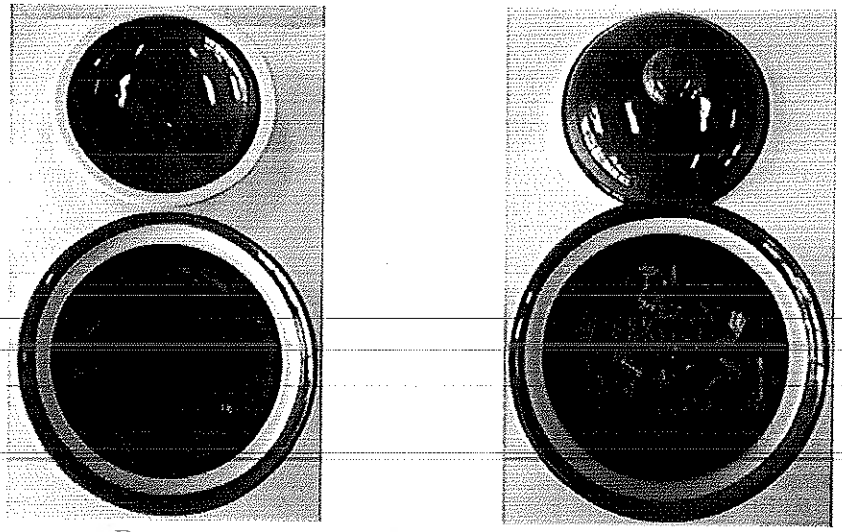

Bagasse Coconut fibre

Figure 4.2 The pristine biochar products (Cont.)

4.1.2 The morphology surface of biochar

SEM analysis of CCB

The SEM pictures of CCB synthesised under different conditions are shown in Figure 10. The surface morphology of biochars had longitudinal pores with the width in the range of 4 – 36.5 μm (Table 4.2).

CCB400 ^{0}C-6 h had mainly large sized pores. At this stage of carbonization, the volatile matter was lost in significant amounts and formed pore openings (Fu et al., 2009), whereas CCB500 ^{0}C-6 h had some changes and multiple pore sizes. The small portion of the volatile matter in biochar was lost gradually, bringing about the numerous pore sizes at 500 ^{0}C (Fu et al., 2009).

When the pyrolysis temperature rose, the surfaces of CCB synthesised in 2, 4, and 6 h at 600 ^{0}C formed several small rough pores. At 600 ^{0}C, the dissolution of only one small part of the remaining volatile matter in the biochar led to the improvement of porosity (Fu et al., 2009). The small pores in the hive formed with approximately 4-5 μm in width were found in CCB600 ^{0}C-4 h. At high temperatures in the pyrolysis process, some pores of CCB600 ^{0}C-6 h were destroyed, due to the long residence time. The biochar pore structures in the high temperatures of the pyrolysis process lead to the melting and breaking of the biochar pores (Yavari et al., 2015). Whereas the surface of non-modified biochar 600 ^{0}C-6 h was observed, minerals were found on the surface of the biochar. The minerals that persisted on the surface of the biochar, led to the blocking of the biochar surface and a decrease in the specific surface area of the biochar.

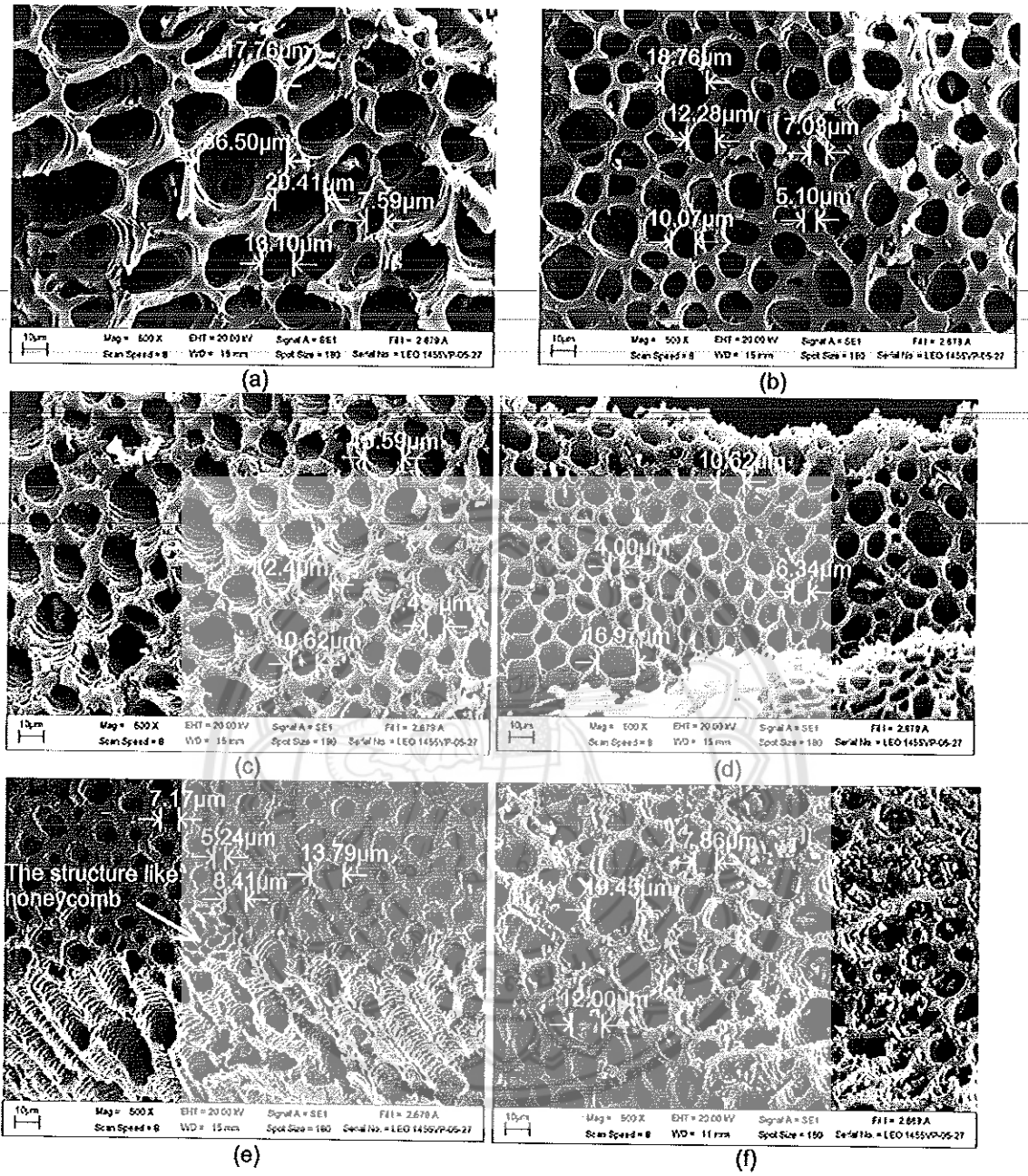

Figure 4.3 SEM of CCB synthesised under different pyrolysis conditions: (a) 400 ^{0}C-6 h, (b) 500 ^{0}C-6 h, (c) 600 ^{0}C-6 h, (d) 600 ^{0}C-2 h, (e) 600 ^{0}C-4 h, (f) 600 ^{0}C-6 h (non- modified)

Table 4.2 The range of pore size of CCB synthesised under different pyrolysis conditions

CCB	The range of pore size (μm)
400 ^{0}C-6 h	7.59 – 36.50
500 ^{0}C-6 h	5.10 – 18.76
600 ^{0}C-6 h	7.45 – 15.59
600 ^{0}C-2 h	4.00 – 16.97
600 ^{0}C-4 h	5.24 – 13.79
600 ^{0}C-6 h (non-modified)	7.86 – 19.45

SEM analysis of BAB

The SEM picture of different BAB is shown in Figure 4.4 For biochar synthesised for 6 h, when the pyrolysis temperature increased from 400 ^{0}C to 600 ^{0}C, the morphology of biochar width tended to be narrow. The width range of BAB400 ^{0}C-6 h was approximately 7.45 – 20.69 μ m. They considered that in this condition, biochar formed pore openings (Fu et al., 2009). Whereas the pores in BAB500 ^{0}C-6 h are of various sizes. The small amount of volatile matter in the biochar was slowly lost, this formed the various pore sizes at 500 ^{0}C (Fu et al., 2009).

When biochar was burned at 600 ^{0}C for 6 h, the total dissolution of small parts of the volatile matter that remained in the biochar was achieved. This brought about the advantage for the formation of the pore of BAB. Where the biochar was burned at different holding times at 600 ^{0}C, the result was the formation of similar biochar pore widths (Figure 4.4 and Table 4.3).

The BAB showed that the pores on the surface of the biochar are longitudinal in shape, which indicates that BAB can take up pollutants by a pore-filling mechanism.

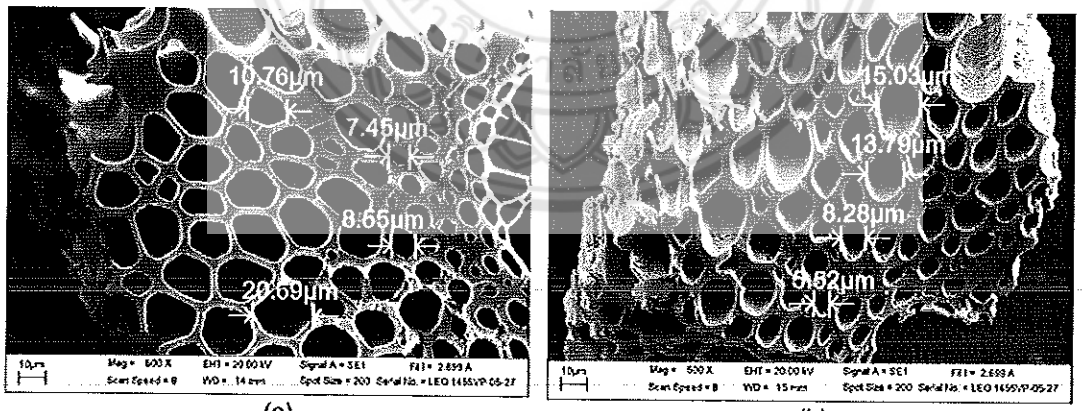

(a) (b)

Figure 4.4 SEM of BAB synthesised under different pyrolysis conditions: (a) 400 ^{0}C-6 h, (b) 500 ^{0}C-6 h, (c) 600 ^{0}C-6 h, (d) 600 ^{0}C-2 h, (e) 600 ^{0}C-4 h

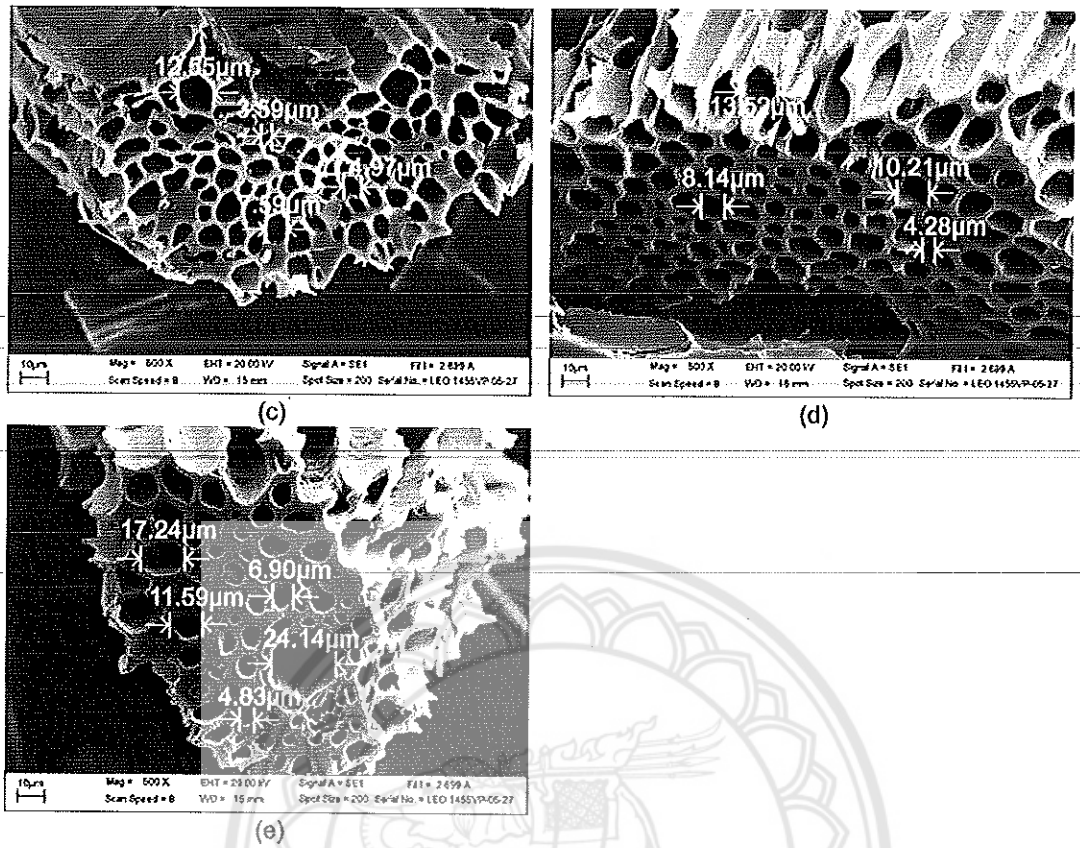

(c) (d)

(e)

Figure 4.4 SEM of BAB synthesised under different pyrolysis conditions: (a) 400 ^{0}C-6 h, (b) 500 ^{0}C-6 h, (c) 600 ^{0}C-6 h, (d) 600 ^{0}C-2 h, (e) 600 ^{0}C-4 h (Cont.)

Table 4.3 The range of pore size of BAB synthesised under different pyrolysis conditions

BAB	The range of pore size (μ m)
400 ^{0}C-6 h	7.45 – 20.69
500 ^{0}C-6 h	5.52 – 15.03
600 ^{0}C-6 h	3.59 – 12.55
600 ^{0}C-2 h	4.28 – 13.52
600 ^{0}C-4 h	4.83 – 17.24

SEM analysis of RHB

The SEM image of RHB is synthesised under different conditions as shown in Figure 4.5 The range of the pore widths of RHB were 1.52 to 19.31 μm as presented in Table 4.4 The pores of RHB formed as vertical and narrow. The structure of biochar depended significantly on the structure of the biomass (Yavari et al., 2015). Probably, the thin structure of rice husk biomass influenced the formation of the pore of biochar (Yavari et al., 2015). The inside of the pores of RHB was a rough structure and was amorphous shape. Therefore, the pore of the RHB can participate in the pore-filling mechanism in the adsorption process.

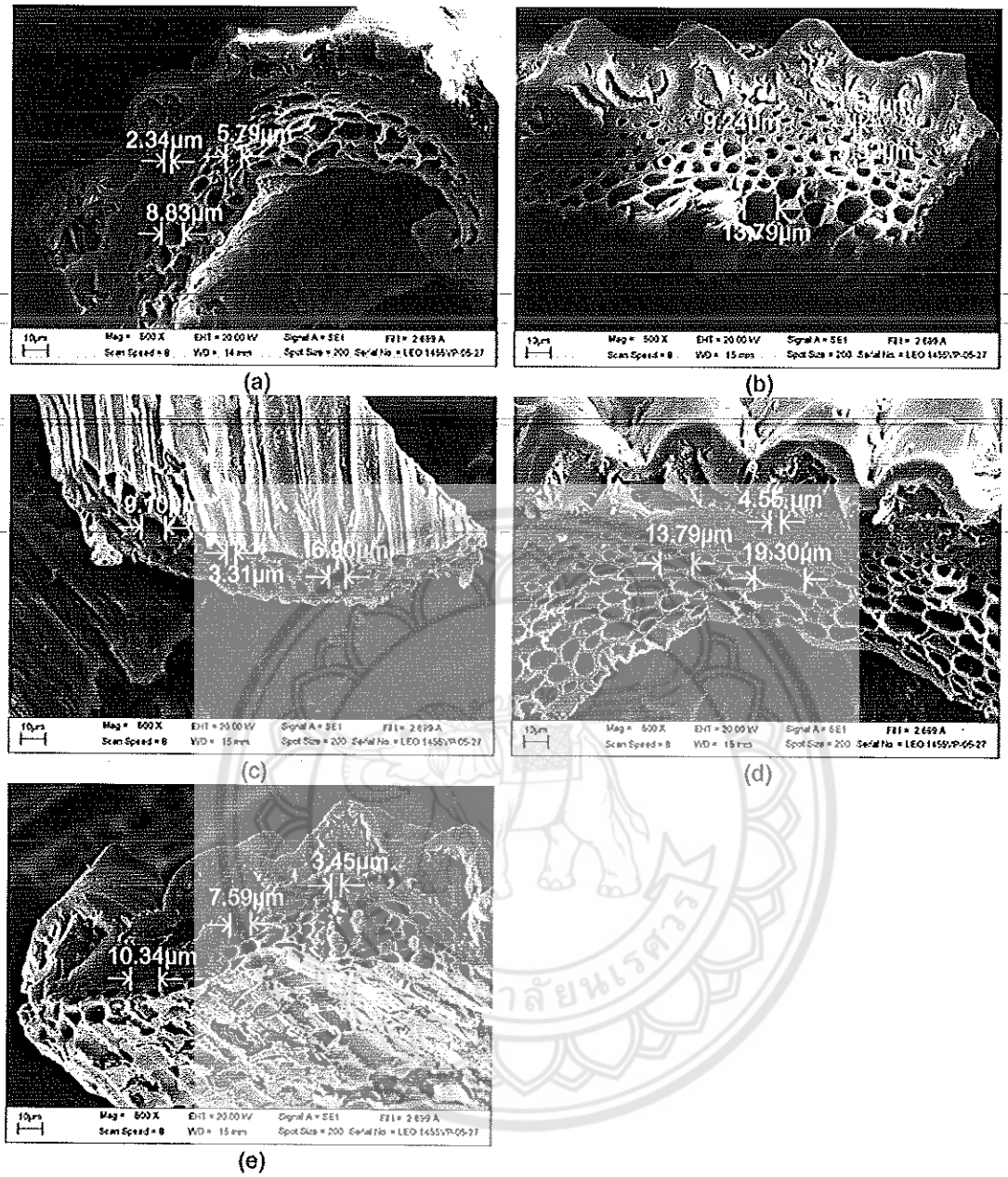

Figure 4.5 SEM of RHB synthesised under different pyrolysis conditions: (a) 400 ^{0}C-6 h, (b) 500 ^{0}C-6 h, (c) 600 ^{0}C-6 h, (d) 600 ^{0}C-2 h, (e) 600 ^{0}C-4 h

Table 4.4 The range of pore size of RHB synthesised under different pyrolysis conditions

RHB	The range of pore size (μ m)
400 ^{0}C-6 h	2.34 – 8.83
500 ^{0}C-6 h	1.52 – 13.79
600 ^{0}C-6 h	3.31 – 9.10
600 ^{0}C-2 h	4.55 – 19.31
600 ^{0}C-4 h	3.45 – 10.34

SEM analysis of CFB

The SEM micrograph of CFB were synthesised under different conditions as presented in Figure 13. The pore structure of CFB were longitudinal pores which the pore widths were in the range of 2.90 to 15.86 μm (Table 4.5).

The pores of CFB400 ^{0}C-6 h were largest size pore when it compared with other CFB (Table 4.5 and Figure 4.6). Synthesis conditions at 400 ^{0}C in 6 h, high amounts of volatile matter were lost and this caused the beginning of the formation of the pores of biochar (Fu et al., 2009). Therefore, the larger pore size was formed in CFB at 400 ^{0}C for 6 h. The SEM pictures of CFB that synthesised at 500 ^{0}C for 6 h and CFB synthesised at 600 ^{0}C for 2 h to 6 h illustrated similarity (Figure 4.6 and Table 4.5). Their pores are smaller than the pore width of CFB400^{0}C-6 h. Because, only a small part of the volatile matter in these biochar were exhausted, leading to the improvement of porosity (Fu et al., 2009). The tiny pores and longitudinal structures were likely due to show a high adsorption capacity of biochar with pollutants.

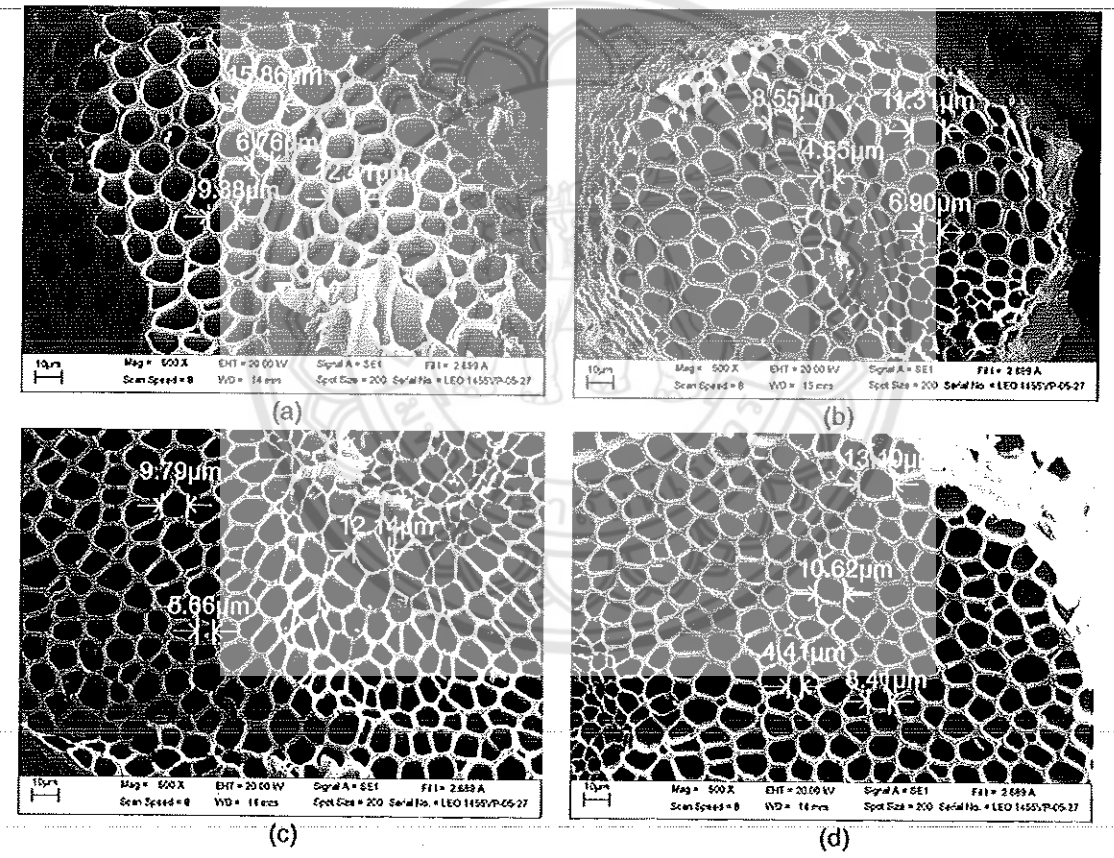

Figure 4.6 SEM of CFB synthesised under different pyrolysis conditions: (a) 400 ^{0}C-6 h, (b) 500 ^{0}C-6 h, (c) 600 ^{0}C-6 h, (d) 600 ^{0}C-2 h, (e) 600 ^{0}C-4 h

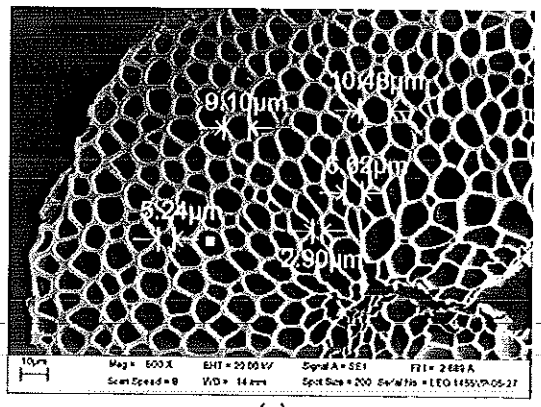

(e)

Figure 4.6 SEM of CFB synthesised under different pyrolysis conditions: (a) 400 ^{0}C-6 h, (b) 500 ^{0}C-6 h, (c) 600 ^{0}C-6 h, (d) 600 ^{0}C-2 h, (e) 600 ^{0}C-4 h (Cont.)

Table 4.5 The range of pore size of CFB synthesised under different pyrolysis conditions

CFB	The range of pore size (μ m)
400 ^{0}C – 6 h	6.76 – 15.86
500 ^{0}C – 6 h	4.55 – 11.31
600 ^{0}C – 6 h	5.66 – 12.14
600 ^{0}C – 2 h	4.14 – 13.10
600 ^{0}C – 4 h	2.90 – 10.48

4.1.3 The determination of SSA and TPV of CCB

The adsorption capacity of biochar is related to the specific surface area. Generally, the high specific surface area (SSA) of biochar led to increasing the adsorption capacity (Guo & Lua, 1998). The SSA of CCB depended on the pyrolysis temperature and holding time as shown in Table 4.6 When CCB was synthesised at 400 ^{0}C and in 6 h, the SSA of CCB was 6.10 m^2/g, at this temperature, the pyrolysis reactions were just beginning to lead to low SSA, although the holding time was 6 h. This was due to the imperfection of heat energy in ejecting volatile materials (Guo & Lua, 1998). When the pyrolysis temperature was increased to 500 ^{0}C and 600 ^{0}C in 6 h, the SSA of CCB was 109.84, and 303.36 m^2/g, respectively. This explains that at high temperatures, the releasing of volatile matter during pyrolysis led to the formation and increase of the surface area.

For CCB burnt at 600 ^{0}C in different holding times, the CCB600 ^{0}C-4 h had a SSA higher than the SSA of CCB600 ^{0}C-2 h (Table 7). The long-term of the holding times enhanced the SSA of biochar, this phenomenon is due to the completion of the carbonization process in biochar which led to the increase of the SSA (Yavari et al., 2015). However, when biochar was synthesised at 600 ^{0}C for 6 h, the SSA of the biochar decreased to 303.36 m^2/g. Some pores were shrinking and were destroyed, leading to the decrease of the SSA. This agrees with previous results (Guo & Lua, 1998), (Chun et al., 2004).

The total pore volume (TPV) is one of the major impacts on the adsorption capacity of biochar. The effects of the pyrolysis temperature and holding time on the TPV of CCB were shown in Table 4.6 The TPV of CCB as synthesised at 400 ^{0}C over 6 hours was quite low. At 400 ^{0}C, the reaction of the pyrolysis process had just begun (Guo & Lua, 1998). On the other hand, the significant loss of volatile matter and the formation of pore openings were just

starting (Fu et al., 2009), therefore this phenomenon conducted the low TPV of CCB400 ^{0}C-6 h. When the pyrolysis temperatures were increased from 500 ^{0}C to 600 ^{0}C, high amounts of volatile matter were exhausted. This gradually led to improved porosity, where the TPV of CCB increased gradually (Guo & Lua, 1998). The TPV of the CCB were increased during pyrolysis from 400 ^{0}C to 600 ^{0}C in 6 h. However, the TPV of CCB600 ^{0}C-6 h was lower than the TPV of CCB600 ^{0}C-4 h, the event was probably due to sintering of the biochar when the holding time was excessive (Guo & Lua, 1998).

Table 4.6 The specific surface area (SSA) and the total pore volume (TPV) of CCB

CCB	SSA (m^2/g)	TPV (cm^3/g)
400 ^{0}C-6 h	6.10	0.0019
500 ^{0}C-6 h	109.84	0.0436
600 ^{0}C-6 h	303.36	0.1131
600 ^{0}C-4 h	350.22	0.1335
600 ^{0}C-2 h	280.67	0.1079

4.2 The selection of good biochar through the comparison of the Q_0

The main factor affecting the Q_0 of biochar is the pyrolysis conditions in burning process of the biochar. The most effective biochar was chosen by the comparison of the Q_0. The four kinds of biochar with comparison of the Q_0 are shown in the following sections:

4.2.1 Comparison the CCB by the Q_0

Figure 14a shows the effect of pyrolysis temperature on the Q_0 of CCB. The burning temperature of biochar increased from 400 ^{0}C to 600 ^{0}C in 6 h and the Q_0 increased from 6.11 to 13.79 mg/g. The high pyrolysis temperature improved the morphology of the surface area (Figure 10), TPV, and SSA of CCB (Table 4.7). Moreover, the adsorption ability of biochar depended significantly on the TPV and SSA (Wang et al., 2018). The TPV and SSA data of CCB increased in the order 400<500<600 ^{0}C in 6 h (Table 4.7), these results led to an increased Q_0, when the burning temperature of biochar increased from 400 ^{0}C to 600 ^{0}C in 6 h. From the results, the high value of TPV and SSA of CCB can be the adsorption of high amounts of atrazine pollutant. The increasing value of TPV and SSA were likely due to the increasing of adsorption sites in biochar. Hence, when the pyrolysis temperature increased, and the Q_0 of CCB increased.

The Q_0 of CCB synthesised from 2 to 5 h at 600 ^{0}C were in the range of 11.73 - 16.22 (mg/g) (Figure 4.7b and Table 4.7). These results are explained through an increase of the value of TPV and SSA of biochar. The adsorption ability of biochar was strongly influenced by TPV and SSA (Wang et al., 2018). The TPV and SSA of CCB were increased by the holding time from 2 to 4 h in the pyrolysis process (Table 4.7). The high value of TPV and SSA were likely due to more sites for atrazine adsorption in the biochar and this led to the increasing of Q_0. However, after 5 h of holding time, the Q_0 of CCB600 ^{0}C-6 h was decreased to 13.79 (mg/g), the TPV and SSA of CCB600 ^{0}C-6 h were decreased in 303.36 m^2/g, 0.1131 cm^3/g, respectively. The decreasing of the Q_0 was proved by the decreasing of TPV and SSA of CCB600 ^{0}C-6 h. Because of a long holding time in the synthesised process, the porous structure of CCB was destroyed, thus the SSA decreased (Yavari et al., 2015). Therefore, the increase of holding time in the biochar synthesised process led to the increasing of the Q_0. However, if the holding time was too long, the Q_0 of the CCB decreased.

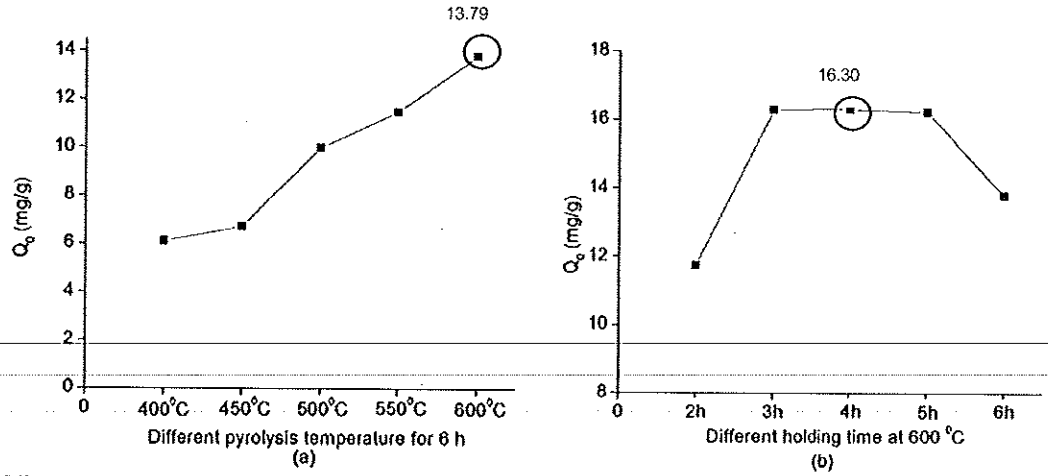

Figure 4.7 The effect of pyrolysis conditions on the Q_0 of CCB: (a) The pyrolysis temperature, (b) The heating time (dosage of CCB = 1.5 g/L, [Atz] = 10-25 mg/L, equilibration time = 48 h)

Table 4.7 The Q_0 of CCB synthesised under different pyrolysis conditions

Biochar	Different pyrolysis temperature for 6 h					Different holding time at 600 ^{0}C				
	400^{0}C	450^{0}C	500^{0}C	550^{0}C	600^{0}C	2h	3h	4h	5h	6h
Q_0 (mg/g)	6.11	6.70	9.99	11.48	13.79	11.73	16.28	16.30	16.22	13.79

4.2.2 Comparison the RHB by the Q_0

Figure 15a shows the influencing of pyrolysis temperature on the Q_0 of RHB. The Q_0 increased from 10.10 to 14.00 mg/g, when biochar was synthesised from 400 to 500 ^{0}C in 6 h (Table 9). This explains that the increasing of the pyrolysis temperature due to enhance the SSA (Guo & Lua, 1998). The adsorption ability of biochar depended on the TPV and SSA significantly (Wang et al., 2018).

However, the pyrolysis process was performed from 550 ^{0}C to 600 ^{0}C in 6 h, the Q_0 of biochar decreased from 11.2k0 to 9.50 mg/g. Probably, at 550 ^{0}C to 600 ^{0}C, the SSA of biochar could decresea due to the high temperature led to the change in form of the pores of the biochar (Yavari et al., 2015). This caused the reduction in the Q_0 of RHB that synthesised at 550 ^{0}C to 600 ^{0}C in 6 h.

The Q_0 of RHB synthesised from 2 to 4 h at 600 ^{0}C was in the range of 9.20 - 11.20 (mg/g) (Figure 15 and Table 9). Possibly, this was expounded through the dissolution of the volatile matter. When the holding time increased, there remains of a small amount of the volatile matter was released causing increasing the SSA and Q_0 (Fu et al., 2009). Nevertheless, the Q_0 of RHB decreased at the synthesis condition at 600 ^{0}C in 6 h. High temperatures and prolonged holding time could cause decreasing the SSA and Q_0 (Yavari et al., 2015).

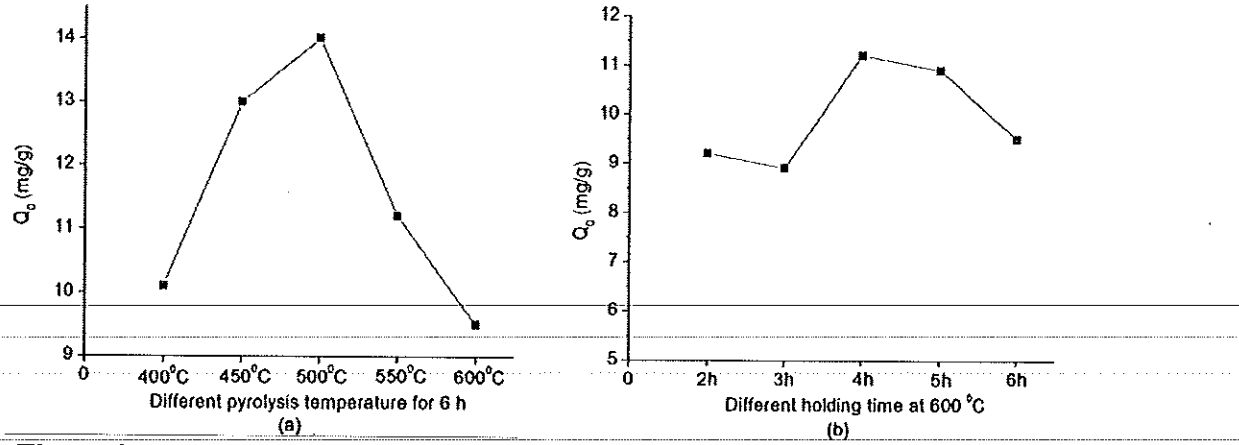

Figure 4.8 The effect of pyrolysis conditions on the Q_0 of RHB: (a) The pyrolysis temperature, (b) The heating time (dosage of RHB = 1.5 g/L, [Atz]: 10-25 g/L, equilibration time = 48 h)

Table 4.8 The Q_0 of RHB synthesised under different pyrolysis conditions

Biochar	Different pyrolysis temperature for 6 h					Different holding time at 600 ^{0}C				
	400^{0}C	450^{0}C	500^{0}C	550^{0}C	600^{0}C	2h	3h	4h	5h	6h
Q_0 (mg/g)	10.10	13.00	14.00	11.20	9.50	9.20	8.90	11.20	10.90	9.50

4.2.3 Comparison the BAB by the Q_0

The results of the pyrolysis temperature effected on the Q_0 of BAB shown in Figure 16a and Table 10. The biochar was synthesised from 400 to 600 ^{0}C in 6 h, the Q_0 increased from 9.50 to 15.50 mg/g (Figure 16a and Table 10). This is due to increasing the pyrolysis temperature to raise the specific surface area (Guo & Lua, 1998). The adsorption ability of biochar depended on the high SSA (Wang et al., 2018).

The influencing of the holding time on Q_0 of BAB as shown in Figure 16b and Table 10. Q_0 of BAB is synthesised from 2 to 6 h at 600 ^{0}C was in the range of 12.20 - 15.50 (mg/g). Possibly, this is related to the dissolution of volatile matter. When the holding time increased, the remains of a small amount of volatile matter was exhausted leading to the augmentation of SSA and Q_0 (Fu et al., 2009).

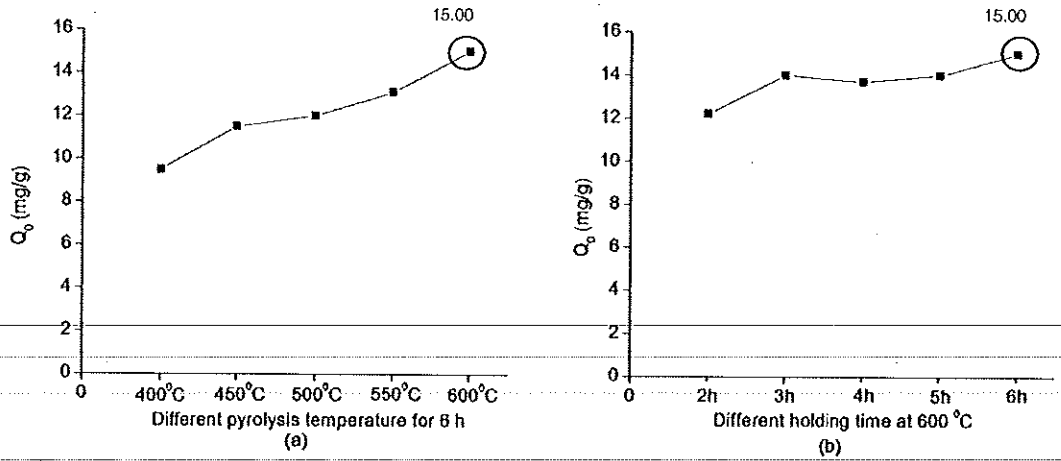

Figure 4.9 The effect of pyrolysis conditions on the Q_0 of BAB: (a) The pyrolysis temperature, (b) The heating time (dosage of BAB = 1.5 g/L, [Atz]: 10-25 g/L, equilibration time = 48 h)

Table 4.9 The Q_0 of BAB synthesised under different pyrolysis conditions

Biochar	Different pyrolysis temperature for 6 h					Different holding time at 600 ^{0}C				
	400^{0}C	450^{0}C	500^{0}C	550^{0}C	600^{0}C	2h	3h	4h	5h	6h
Q_0 (mg/g)	9.50	11.50	12.00	13.1	15.00	12.20	14.00	13.7	14.0	15.00

4.2.4 Comparison the CFB by the Q_0

The effect of pyrolysis temperatures and holding times on the maximum adsorption capacities of CFB are illustrated in Figure 17 and Table 11. For the effect of pyrolysis temperatures on the Q_0, the Q_0 of the biochar was achieved at 550 ^{0}C in 6 h (128.70 mg/g). The Q_0 of biochar that was pyrolysed at 400 ^{0}C and
550 ^{0}C was augmented from 18.90 to 128.70 mg/g. This suggests that increasing the pyrolysis temperature would argument the specific surface area (Guo & Lua, 1998). The high SSA brings about a high adsorption capacity of biochar (Wang et al., 2018).

For the effect of holding times on the Q_0, the Q_0 of biochar was succeeded at 600 ^{0}C in 4 h (141.70 mg/g), this is clarified as the effect of pyrolysis temperatures on the Q_0. The value of Q_0 was slightly decreased as observed in CFB at 600 ^{0}C in 6 h. Possibly, the longer holding time at high temperature in the pyrolysis process causes the decreased specific surface area of CFB (Yavari et al., 2015). This result is similar to the result of CCB.

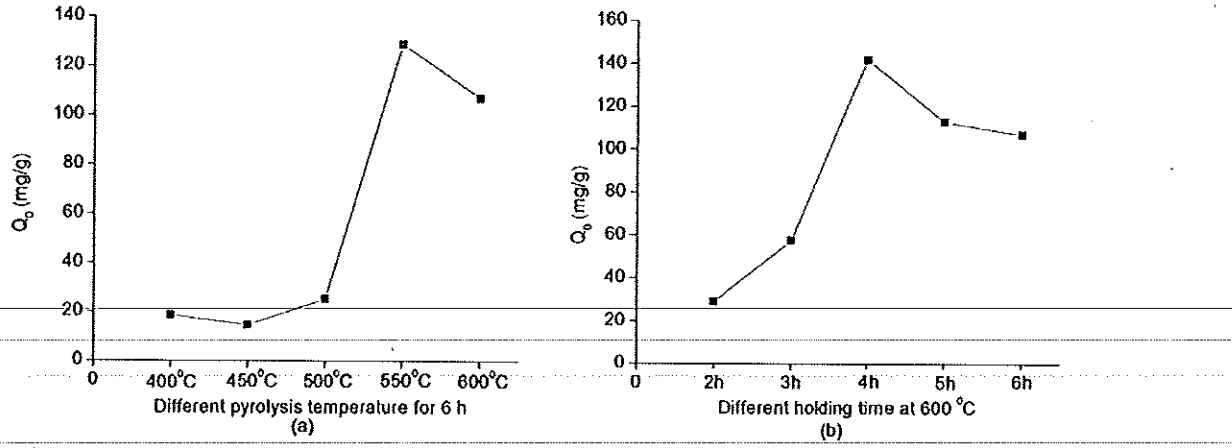

Figure 4.10 The effect of pyrolysis conditions on the Q_0 of CFB: (a) The pyrolysis temperature, (b) The heating time (dosage of CFB = 1.5 g/L, [Atz]: 10-25 g/L, equilibration time = 48 h)

Table 4.10 The Q_0 of CFB synthesised under different pyrolysis conditions

Biochar	Different pyrolysis temperature for 6 h					Different holding time at 600 ^{0}C				
	400^{0}C	450^{0}C	500^{0}C	550^{0}C	600^{0}C	2h	3h	4h	5h	6h
Q_0 (mg/g)	18.90	14.70	25.40	128.70	107.00	28.90	57.40	141.70	112.90	107.00

4.3 Characterization analysing of the optimum of four kinds of biochar

4.3.1. The pHpzc of the optimum biochar

The pHpzc values of the four kinds of biochar (CCB600 ^{0}C-4 h with HF modification: (CCB), RHB500 ^{0}C-6 h with HF modification: (RHB), BAB600 ^{0}C-6 h with HF-H_2SO_4 modification: (BAB), CFB 600 ^{0}C-4 h with HCl modification: (CFB)) were from 0.7 to 0.75 and are indicated in Figure 18. They show that a positive charge will generate on biochar surface, when the pH of the solution is lower than pHpzc values. If the solution has pH higher than the pHpzc values, the biochar surface will be negatively charged (N. Liu et al., 2016).

The pHpzc of biochar results (0.7 - 0.75), shows that the pH range varies greatly, and expresses the electrostatic interactions which may occur between biochar and pollutants when the pH of the solution is higher than pHpzc values (Komnitsas, Zaharaki, Bartzas, & Alevizos, 2017). The pHpzc values of the biochar, as illustrated, shows high adsorption proficiency of pollutants in the anionic form (Hafshejani et al., 2016).

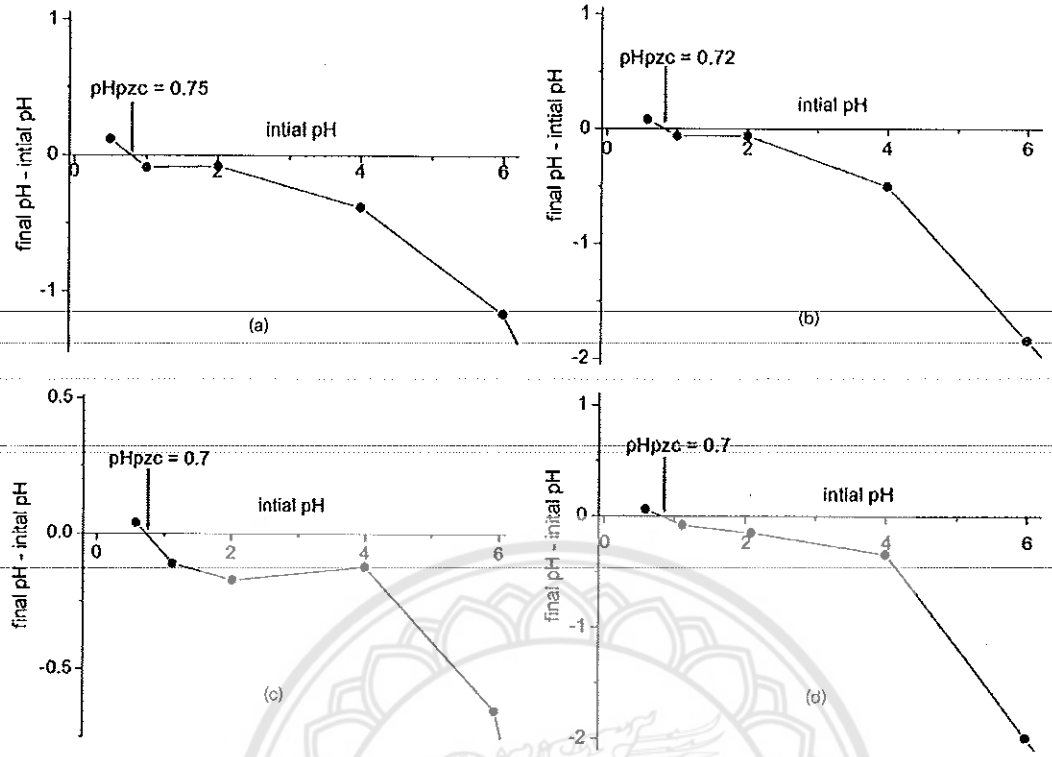

Figure 4.11 pHpzc values of the optimum biochar: (a) CCB, (b) RHB, (c) BAB, (d) CFB

4.3.2. Specific surface area and total pore volume of the optimum biochar

The specific surface area (BET) and total pore volume (TPV) of the four kinds of biochar are shown in Table 12. Table 12 indicates that the specific surface area of CFB and CCB are higher than those of RHB and BAB. The original biomass and the pyrolysis conditions influenced the physical and chemical properties of biochar (Yavari et al., 2015), this also affected the specific surface area (BET) of the biochar. Morever, the biomass original structure is due to the determination of the porosity structure and the specific surface area of the biochar (Yavari et al., 2015). If the large specific surface area exists on the surface of the biochar, it has more interfaces for pollutant adsorption (G. Tan et al., 2016).

The pore size of the biochar played an important role in pore-filling adsorption. The pore size distributions of the four kinds of biochar are presented in Table 12. The pore volume distributions (%) in pore sizes of micropores (< 2 nm) and narrow mesopores (2-20 nm) were in the range of 7.90 - 21.24 % and 56.57 - 69.22 %, respectively. The pore size of the biochar is very important in performing the uptake of the adsorbate (Wang et al., 2018).

Table 4.11 The specific surface area (SSA), the total pore volume (TPV), and the pore size distributions (%) of biochars

Biochar	SSA (m^2/g)	TPV (cm^3/g)	The pore size distributions (%) of biochars			
			Micropores (< 2 nm)	Narrow mesopores (2-20 nm)	Mesopores (21-50 nm)	Macropores (> 50 nm)
CCB	292.92	0.117	21.24	56.57	10.39	11.81
RHB	153.27	0.055	7.90	59.26	13.97	18.87
BAB	67.42	0.029	16.88	59.29	15.75	8.07
CFB	402.43	0.151	17.40	69.22	6.10	7.28

4.3.3. The acid and base functional groups of the optimum biochar

The values of the acid and base functional groups of the biochars by Boehm titrations method are shown in Table 13. The total acidity of RHB and CFB were higher than those of CCB and BAB. The total basicity of the biochar are similar (Table 13). The total acidity is defined by oxygenated groups including carboxyl, lactonic, and phenolic. Whereas, the surface base functional group are presented by the ketone group. Both of the acid and base functional groups can act as the efficiency adsorption sites for pollutant removal (Hai Liu et al., 2015).

Table 4.12 The surface chemistry of the biochars

Biochar	Carboxyl (mmol/g)	Lactonic (mmol/g)	Phenolic (mmol/g)	Total acidity (mmol/g	Total basicity (mmol/g)
CCB	0.250	0.250	0.250	0.750	0.285
RHB	0.500	0.400	0.500	1.400	0.285
BAB	0.200	0.100	0.200	0.500	0.228
CFB	0.375	0.250	0.625	1.250	0.285

4.3.4. The hydrophilic properties of the optimum biochar

The hydrophilic property of the four kinds of biochar were tested by the contact angle method. This test indicated that the surface of the four kinds of biochar (CCB, RHB, BAB, and CFB) were totally wet with water ($\theta < 30^0$). This indicates that the four kinds of biochar have significant hydrophilic properties. If biochar has a hydrophilic property, it enables the penetration of water in the pore (Z. Liu et al., 2017). This shows that the advantage of pollutant diffusion is conducted by the intrapores of biochar leading to a high adsorption capacity.

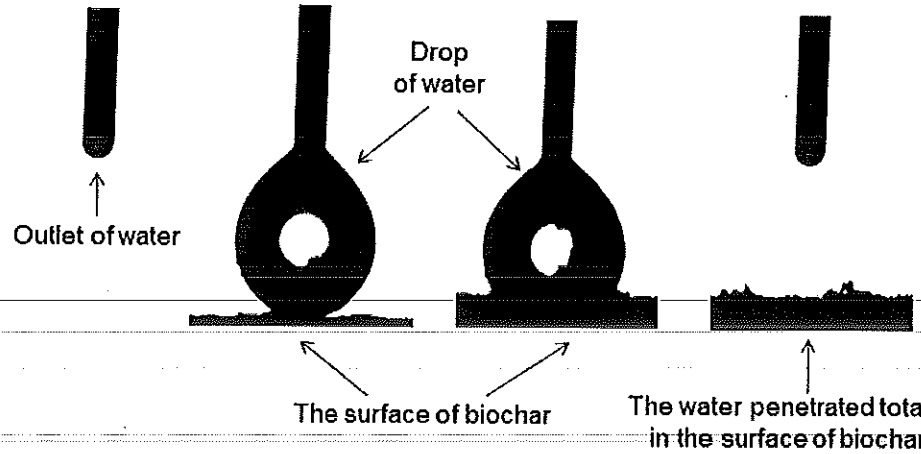

Figure 4.12 The result of the contact angle method of biochar

4.3.5. FT-IR of the optimum biochar

The FT-IR results show the qualitative value of the surface functional groups of biochars. The FT-IR spectra of the biochars are shown in Figure 19 and Table 14. The spectra show the existence of eight major functional groups on the surfaces of the biochars.

The bands around 1216 and 1217 cm^{-1} were ascribed to the aromatic C-O stretching of phenolic hydroxyl (Chun et al., 2004). The bands at around 1045 and 1099 cm^{-1} were ascribed to the aromatic C-O stretching of alcohol (Saffari, Karimian, Ronaghi, Yasrebi, & Ghasemi-Fasaei, 2015). Peaks at around 878 and 719 cm^{-1} were assigned to the aromatic C-H out-of-plane bending mode. These peaks show the aromatic benzene rings presented on the biochar surface (Tran, Wang, You, & Chao, 2017). The peaks at around 2911 and 2845 cm^{-1} were ascribed to C-H stretching of the alkyl group (Kinney et al., 2012). The 3000-3600 cm^{-1} peak area was assigned to the stretching vibration of the hydroxyl groups and presented significant H-bonding interaction (X. Chen et al., 2011). Peaks around 1736 and 1715 cm^{-1} represented the carbonyl group C=O, and they could indicate ketone, carboxylic acid, and ester. These groups are also the indicators of H-bonding interaction (N. Liu et al., 2015).

The bands at 2354 and 2299 cm^{-1} represented ketone groups C=O with stretching vibrations (Nuithitikul et al., 2010). The band areas around 1563 and 1601 cm^{-1} were assigned to the aromatic C=C (Ahmad et al., 2007).

From FT-IR analysis, the major functional groups of the biochars including ketone, carbonyl, and aromatic organic molecules which are unsaturated hydrocarbons. The hydroxyl group is also the predominant molecule on the biochars. All these functional groups can cause H-bonding interactions between the biochars and the pollutants. Additionally, the aromatic functional group of the biochars has the π-π EDA interaction with the pollutants (N. Liu et al., 2015). The alkyl group of biochars have hydrophobic properties (Kinney et al., 2012) and this group can constitute the hydrophobic interaction with pollutants.

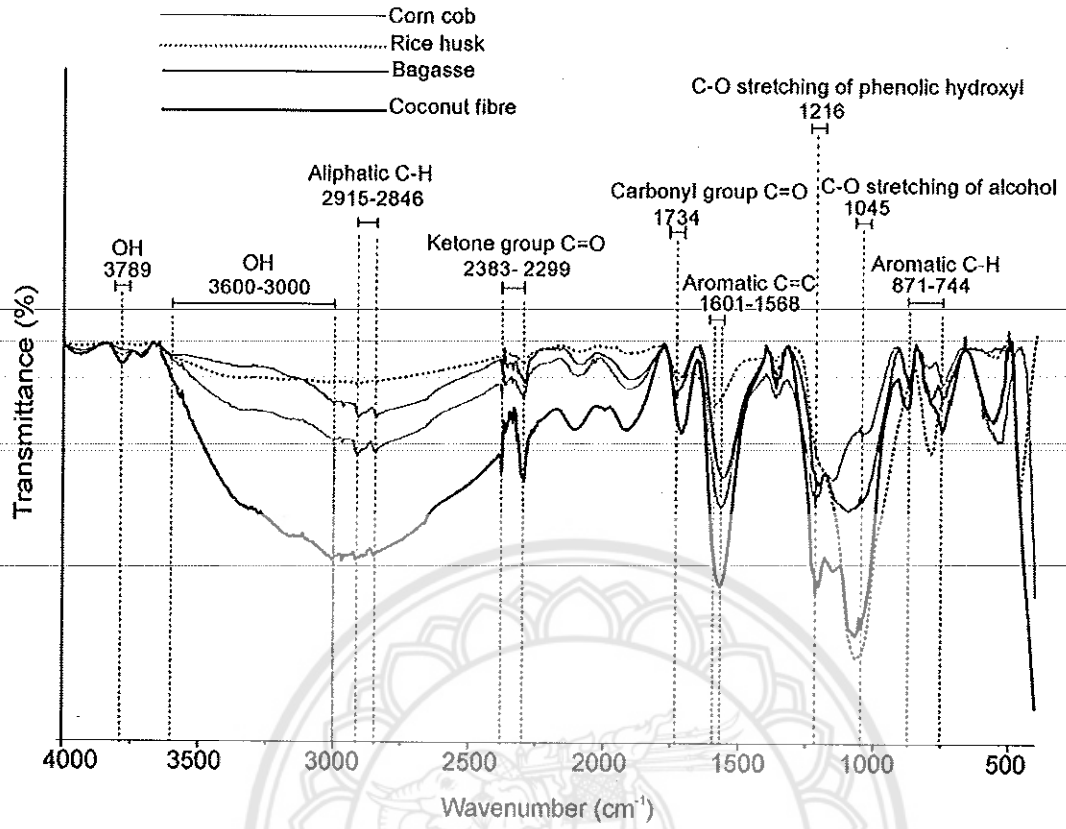

Figure 4.13 FT-IR spectra analysis of the optimum biochar

Table 4.13 FT-IR spectra results of the optimum biochar

The functional groups of biochar	CCB	RHB	BAB	CFB
	Wavenumber (cm^{-1})			
Aromatic C-H	871-744	719	847-748	878-750
C-O stretching of alcohol	1045	1063	1099	1070
C-O stretching of phenolic hydroxyl	1216	-	1216	1217
Aromatic C=C	1568	1601	1563	1571
Carbonyl group C=O	1734	1716	1736	1715
Ketone group C=O	2383-2299	2299	2382-2298	2354-2299
Aliphatic C-H	2915-2846	2915-2845	2911-2845	2915-2845
OH group	3600-3000	3600-3000	3600-3000	3600-3000

4.4 Effect of the biochar dosage and the pH of the solution on pesticide adsorption onto the biochar

4.4.1 Effect of the biochar dosage on pesticide adsorption onto the biochar

Biochar dosage plays a key role in pollutant adsorption efficiency. Figure 21 shows the effect of the dosage of CCB600 ^{0}C-6 h on atrazine removal efficiency. It indicated that the highest removal efficiency of atrazine at biochar dosages of 1.5 g/L was 89.60 %. As the dosage of the biochar is increased from 0.25 to 1.5 g/L, atrazine removal increased from 17.55 % to 89.60 %. However, if the dosage of biochar increased from 2.0 to 8.0 g/L, the atrazine removal was slightly decreased from 88.63 to 81.12 %. The increasing dosage of biochars from 0.25 to 1.5 g/L leads to the increasing percentage of atrazine removal due to the increase in the total active sites of biochar. This result agreed with the report of Tan et al. (2015). However, the increasing of the biochar dosage from 2 to 8 g/L leads to a reduction in the percentage of atrazine removal of biochar due to the aggregation of the biochars (X. Chen et al., 2011).

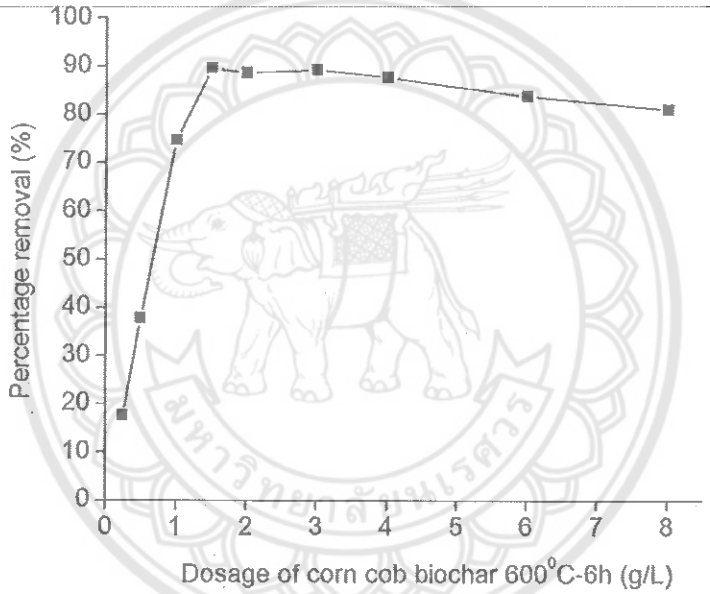

Figure 4.14 Effect of CCB dosage on atrazine adsorption ([Atr] = 10 mg/L, equilibration time = 60 h, pH = 6.5)

4.4.2. The influence of pH on pesticide adsorption onto the biochar

The influence of pH on atrazine adsorption onto the biochar (CCB, RHB, BAB, and CFB)

The values of the pH is a main factor that effects adsorption behaviour (Yue et al., 2017). The pH of the solution influenced the atrazine removal as illustrated in Figure 22 and Table 15. The percentage of highest removal of atrazine by biochars are achieved at a pH of 1.5 and 2.0. This is demonstrated by the ionzation of atrazine (pKa ≈1.68) (Yue et al., 2017) and the change of the charge surface of the biochar. When the pH was adjusted at 1.5 and 2.0 which were approximately similar to the pKa of atrazine (1.68), the atrazine changed in two forms: the cationic form and the non-ionic form (Yue et al., 2017) (Figure 23). Whereas, at these pH levels, the surface charge of the biochar was generated negatively charged, because of the pH of the solution is higher than pHpzc of biochar (pHpzc ≈ 0.7 – 0.75) (N. Liu et al., 2016). The carboxylic acid was considered to convert to carboxylate anions (Essandoh, Wolgemuth, Jr.,

Mohan, & Mlsna, 2017). Therefore, the electrostatic interaction occurred between the negatively charged biochar surfaces and the cationic form of atrazine at pH of 1.5 and 2.0 (Figure 24).

When the pH of the solution was controlled from 4 to 12, the percentage of atrazine removal decreased gradually (Figure 22, Table 15), and the percentage of the lowest removal of atrazine by biochar occurred at pH of 12. This is explained according to when the pH value increased, the cationic proportion of atrazine was reduced (Yue et al., 2017). In addition, as the pH of the solution was higher than the pHpzc of biochars (pHpzc ≈ 0.7 – 0.75), the surface charge of the biochars were negatively charged. Probably, this causes the reduction of the electrostatic interaction between atrazine ions and the surface charge of the biochar. This led to a decrease in the percentage removal of atrazine by the biochar. Moreover, at a high pH (pH > 8), the phenolic hydroxyl groups of biochar increased deprotonation. This was brought about by the rising of the density of negative charges on the biochars (Essandoh et al., 2017), and this also affected the decreasing of the percentage of atrazine removal. Hence, the lowering of the percentage of atrazine removed by the biochar when the pH is higher.

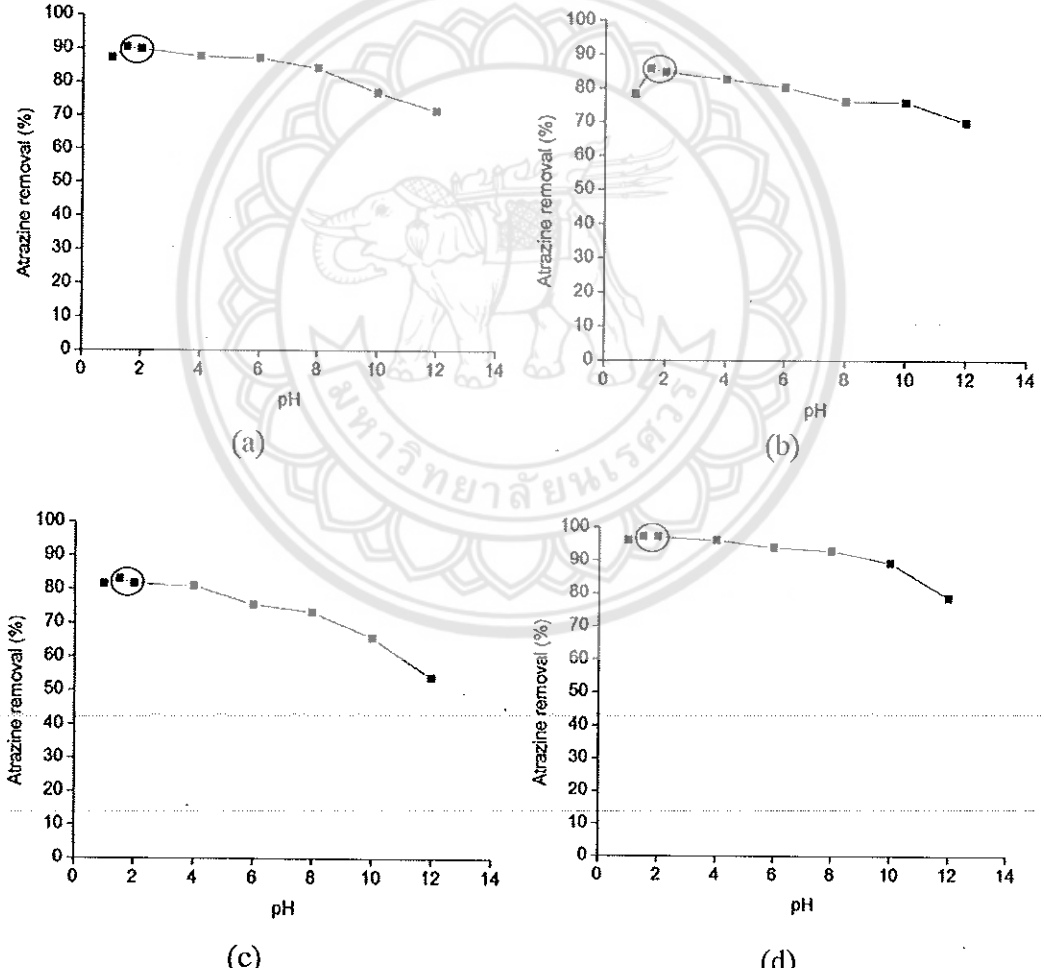

Figure 4.15 The influence of pH on the efficiency of atrazine removal by the biochars: (a) CCB, (b) RHB, (c) BAB, (d) CFB (biochar dosages = 1.5 g/L, [Atz] = 15 mg/L)

Table 4.14 The pH of the solution effected the efficiency of atrazine removal by the biochars

pH	The atrazine removal by biochar (%)			
	CCB	RHB	BAB	CFB
1.0	87.17	78.40	81.56	95.99
1.5	90.32	85.78	83.05	97.27
2.0	89.79	84.71	81.66	97.11
4.0	87.54	82.62	80.97	96.04
6.0	87.12	80.17	75.41	93.85
8.0	84.12	76.10	73.27	92.78
10.0	76.80	75.89	65.57	89.09
12.0	71.40	69.69	53.76	78.62

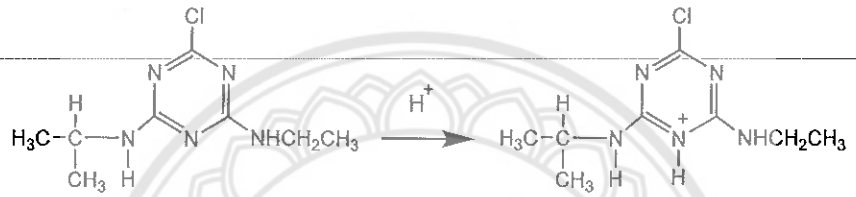

Figure 4.16 Atrazine changed in the cationic form in the acid condition
Sources: (Santos & Masini, 2015)

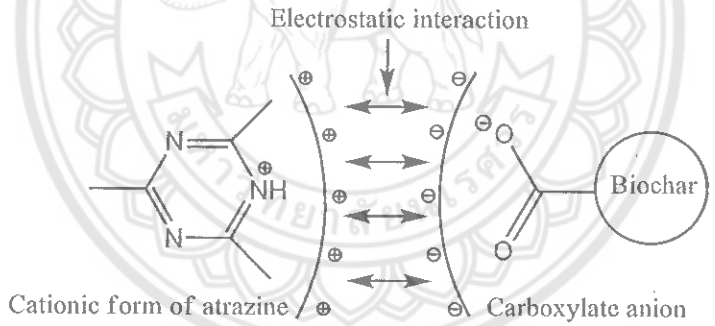

Figure 4.17 The electrostatic interaction between atrazine and biochars around pH of 1.5 and 2.0: the cationic form of atrazine and carboxylate anions on the biochar surface

The influence of pH on 2,4-D adsorption onto the biochar (CCB, RHB, BAB, and CFB)

The pH of solution influenced on the 2,4-D removal by biochars were indicated in Figure 25 and Table 16. The result observed that the efficiency of 2,4-D removal decreased, when the pH values increased. The electrostatic interaction was engendered by the surface of the biochar and 2,4-D, depending on changes in the pH of the solution (Njoku &.Hameed, 2011). The percentage of the highest removal of 2,4-D was succeeded at a pH of 2.0, which was performed by the electrostatic attraction. At a pH of 2, the 2,4-D was formed as positively charged (Njoku & Hameed, 2011), because the pH of the solution is lower than pKa of 2,4-D (2.8) (Herold et al., 2003). While, the surface charge of the biochars are negatively charged, when the pH of the solution is adjusted higher than the pHpzc values of biochar (pHpzc ≈ 0.7 – 0.75) (N. Liu et al., 2016). Hence, at a pH of 2, an electrostatic attraction occurred between the negatively

charged biochar and the positively charged 2,4-D which brought about the highest removal of 2,4-D for biochars.

When the pH of solution were adjusted from 4 to 12, the percentage of 2,4-D removal decreased gradually (Figure 25 and Table 16). This was demonstrated by electrostatic repulsion. When the pH values of the solution is increased (pH > 2.8), the 2,4-D was changed in a large fraction of the anionic form (Njoku & Hameed, 2011). In addition, the surface charge of the biochars were negatively charged, because the pH of the solution were higher than the pHpzc of the biochars (pHpzc ≈ 0.7 – 0.75). Therefore, at a pH from 4 to 12, electrostatic repulsion was generated between the 2,4-D in anionic form and the negatively charged biochar surface, leading to the decrease of 2,4-D removal. This result is similar to the previous work of Essandoh et al. (2017).

In addition, at a pH of 12, the percentage of 2,4-D removal by biochar was the lowest. If the pH of the solution is higher than 8, the phenolic hydroxyl groups of biochar are increased deprotonation, causing the rising the density of negative charges on the biochars (Essandoh et al., 2017). This led to the repulsion that occurred between the phenolate anions of biochar and the carboxylate anion of 2,4-D (Essandoh et al., 2017) (Figure 26a). On the other hand, the carboxylate anions of both biochar and 2,4-D were generated and caused the repulsion between of them (Essandoh et al., 2017) (Figure 26b). Therefore, the pH of the solution was highest, causing the efficiency of the percentage of 2,4-D removal to be the lowest.

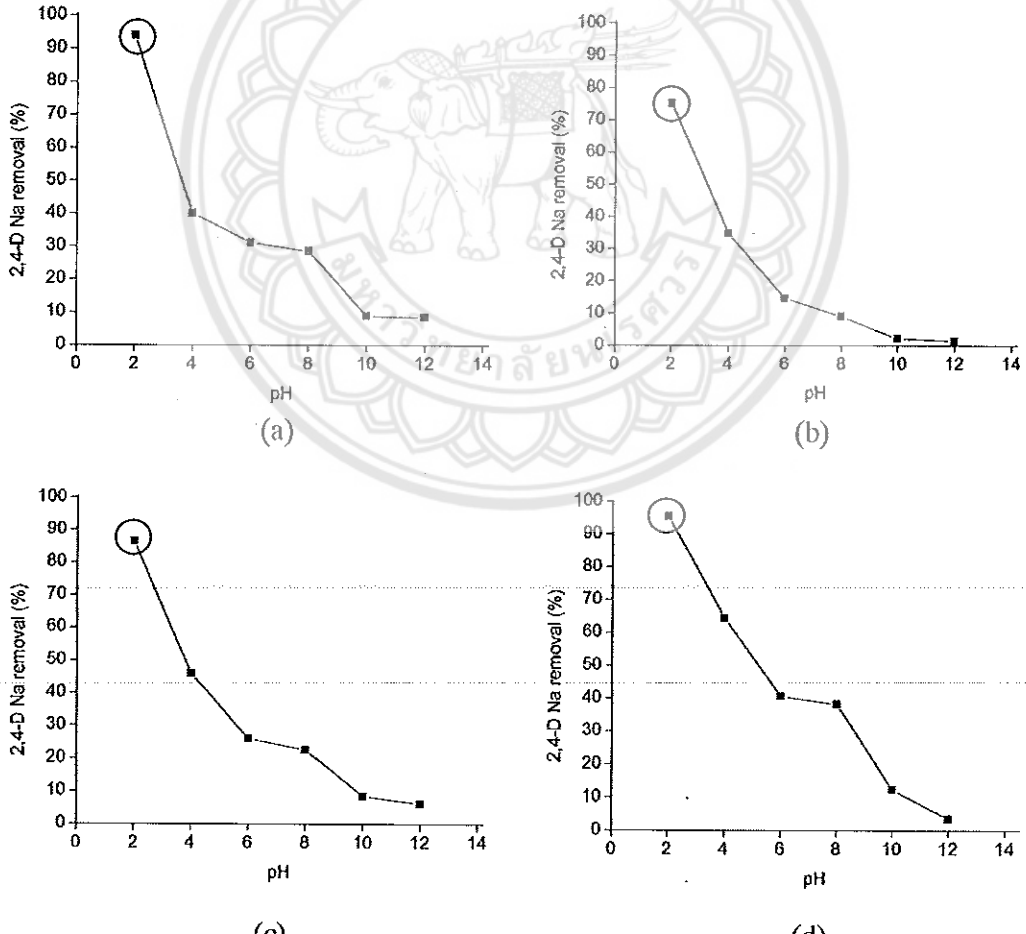

Figure 4.18 The influence of pH on the efficiency of 2,4-D removal by biochars: (a) CCB, (b) RHB, (c) BAB, (d) CFB (biochar dosages = 1.5 g/L, [2,4-D] = 50 mg/L)

Table 4.15 The effect of the pH of the solution on the efficiency of 2,4-D removal by biochars

pH	The 2,4-D removal by biochar (%)			
	CCB	RHB	BAB	CFB
2.0	93.85	75.27	86.45	95.44
4.0	40.06	34.73	45.92	64.38
6.0	31.07	14.67	25.92	40.59
8.0	28.46	9.05	22.60	38.17
10.0	8.82	2.13	8.40	12.37
12.0	8.40	1.36	6.21	3.43

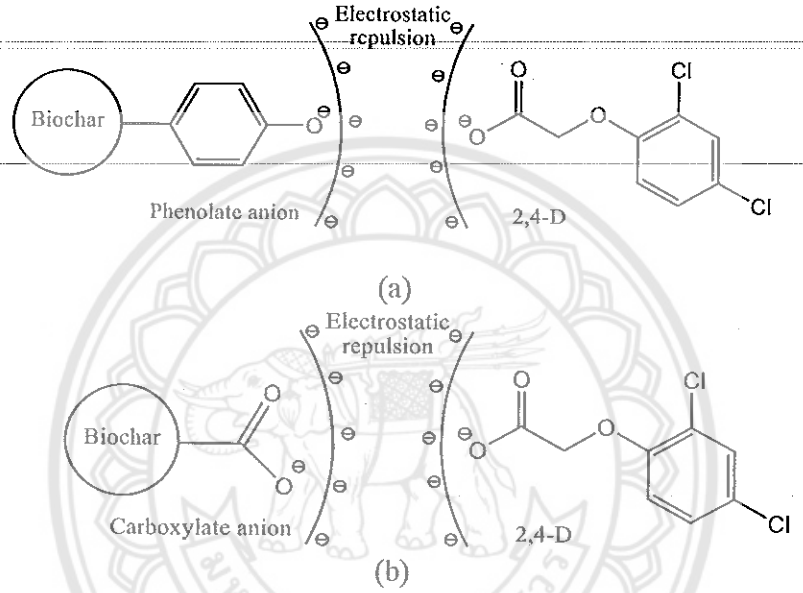

Figure 4.19 The electrostatic repulsion between 2,4-D and biochars at pH ≥ 4: (a) the phenolate anion on the biochar surface and carboxylate anion of 2,4-D, (b) the carboxylate anion on the biochar surface and carboxylate anion of 2,4-D

The influence of pH on pymetrozine adsorption onto the biochar (CCB, RHB, BAB, and CFB)

Figure 27 and Table 17 show the influence of the pH of the solution on the pymetrozine removal using biochar. The ionization constants of pymetrozine is a main factor in controlling the effective removal of pymetrozine depending on the pH of the solution.

The percentage of pymetrozine removal was the highest between pH 3.0 and 4.0 (Figure 27 and Table 17). The formation of the H-bonding interaction around these pH levels were between the H from hydroxyl, and the carboxylic groups of the biochar and the N atom of pymetrozine. At these pH values, as the solution is acidic, the proton (H^+) was added to the N atom (EFSA, 2014), therefore the N atom of the pyridine ring had protonation ($pK_{a2} \approx 4.0$, dissociated 99.4 %), this brought about more electrons that caused a negative charge on the N atom. One of the H-bonding forms was created using an H atom and an electronegative N atom (IUPAC, 2014). In the pyridine ring, the electronegativity of an N atom was higher than the electronegativity of C, this led to a positive charge on the nucleus and a negative charge on the N atom (Sykes, 1985). Carboxylic acid, and phenolic groups of the biochar can generate a hydrogen bond donor (Essandoh et al., 2017). Hence, the H-bonding interaction is formed using

H from carboxyl, phenolic and alcohol groups of the biochar and N atom from the pyridine ring of pymetrozine. The H-bonding interaction mechanism is shown in Figure 28b.

The second high level of pymetrozine removal were observed at a pH of approximately 0.7 (Figure 27 and Table 17). At this pH, the proton (H^+) was added to the N atom 1 of the triazine ring, it led to protonation ($pKa_1 < 1$, dissociated 99.4 %) (EFSA, 2014). The N atom of the triazine ring carried electronegativity, which could have interactions with H from carboxyl, phenolic and alcohol groups of biochar through H-bonding (Figure 28a). Additionally, using the Huckel method to determine the charge of the atoms of pymetrozine was evaluated by the ChemBio3D software. The charge of N atom 2 of the triazone ring showed a negative charge of approximately - 0.17, whereas the charge of N atom of the pyridine ring, had a negative charge of approximately - 0.23. Both N atoms where involved in H-bonding with H from, phenol, alcohol, and carboxyl groups of biochar. From the calculations using the Huckel method, the N atom charge of the pyridine ring, has a higher negativity than the N atom 2 charge of the triazone ring. Therefore, the percentage of pymetrozine removal at pH < 1, is lower than removal in the range of pH of between 3.0 and 4.0 (Figure 27 and Table 17).

When the pH levels were in the range of 6 to 10, the percentage of pymetrozine removal were slightly decreased (Figure 27 and Table 17). Possibly, the increasing of pH values cause the decreasing of the ionization of the pymetrozine, leading to a reduction in the percentage of pymetrozine r
emoval. Probably, at these pH values, the adsorption mechanisms, including pore-filling, π–π EDA, hydrophobic interactions, participate in the removal of pymetrozine.

When the pH levels of the solution were changed to 11.4 or 12, the pymetrozine removal decreased significantly (Figure 27 and Table 17). When the pH of the solution was approximately 11.4 or 12, the N of the triazinone ring had deprotonation, which removed the proton in the amine group of the triazinone ring. The protonation caused N of the triazinone ring carried a positive charge (EURL-SRM, 2016). This did not form the H-bonding interaction between H from the functional groups of biochar, and the N atom from the triazinone ring (Figure 28c). This led to a decrease in the percentage of the pymetrozine removal in the pH value range of 11.4 to 12.

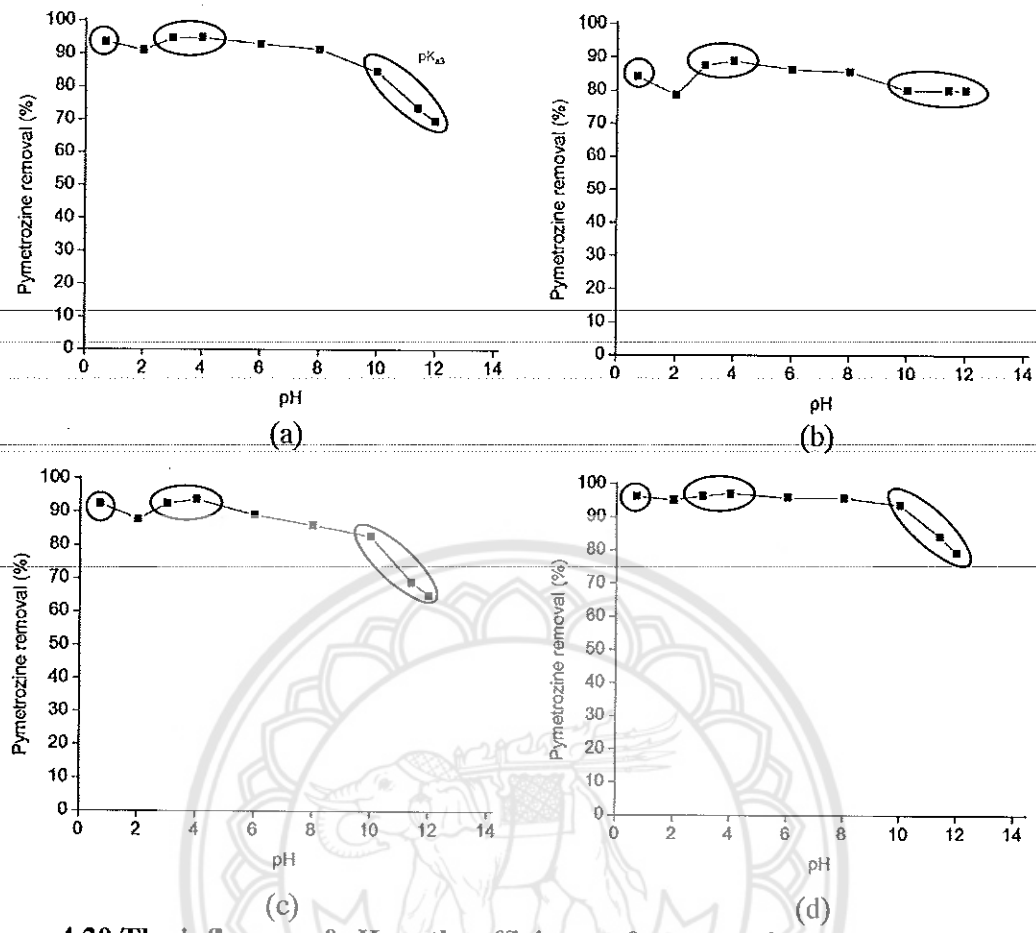

Figure 4.20 The influence of pH on the efficiency of pymetrozine removal by biochar: (a) CCB, (b) RHB (c) BAB, (d) CFB (biochar dosages = 1.5 g/L, [Pym] = 20 mg/L)

Table 4.16 The pH of solution effected on the efficiency of pymetrozine removal by the biochars

pH	The pymetrozine removal by biochar (%)			
	CCB	RHB	BAB	CFB
0.7	93.58	84.09	92.31	96.18
2.0	91.04	78.69	87.80	95.17
3.0	94.75	87.54	92.47	96.34
4.0	94.86	88.87	93.74	97.14
6.0	93.00	86.37	89.02	95.92
8.0	91.41	85.52	85.95	95.76
10.0	84.57	80.12	82.66	93.64
11.5	73.59	80.06	68.88	84.04
12.0	69.51	80.01	64.95	79.22

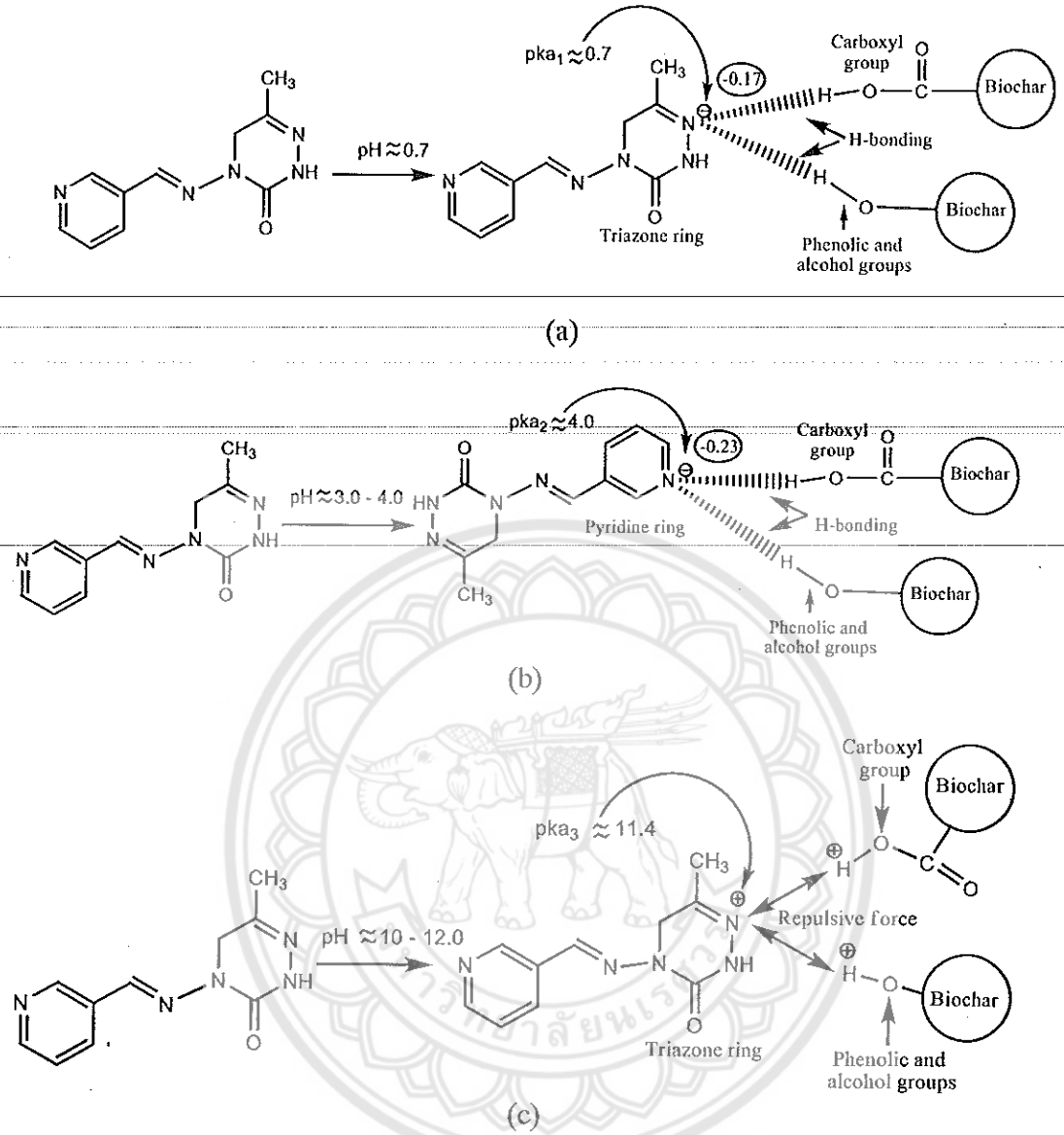

Figure 4.21 The interaction between pymetrozine and biochar: (a) the H-bonding interaction between N from triazone ring and biochar, (b) the H-bonding interaction between N from pyridine ring and biochar, (c) the repulsive force between N from triazone ring and biochar

4.5 Adsorption isotherm models of pesticides adsorbed on the biochar (CCB, RHB, BAB, and CFB)

4.5.1. Adsorption isotherm models

The adsorption isotherms of the pesticides and the biochars that were investigated in this study. Tables 38, 39, 40, and 41 indicated that the Langmuir model and the Freundlich model fitted the experimental data.

Mostly, the Langmuir model was more appropriate than the Freundlich model. The R^2 of the Langmuir model were higher than the R^2 of the Freundlich model (Tables 38, 39, 40, and 41). This showed that monolayer adsorption of pesticides occurred on the surface of the biochars. However, the experimental data of CFB with atrazine, RHB with 2,4-D, and CCB with dichlorvos (Tables

38, 39, and 41) fitted the Freundlich model, this indicated that multilayers and heterogeneous adsorption occurred on the surface of biochars. The data indicated in Tables 38, 39, 40, and 41, the R_L values were higher than 0 and less than 1, it was in the range of 0.0001 to 0.0033 and demonstrated the favorability of the biochars for pesticide adsorptions (Essandoh et al., 2017).

Table 4.17 Isotherm parameters of atrazine adsorption onto the optimum biochars

Models	Parameters	Biochar			
		CCB	RHB	BAB	CFB
Langmuir	Q_0 (mg/g)	19.2	16.1	15.0	18.4
	K_L (L/mg)	0.67	0.67	0.87	3.10
	R_L	0.0021	0.0025	0.0026	0.0022
	R^2	0.985	0.992	0.983	0.976
Freundlich	K_F (mg g^{-1}) (mg L^{-1}) $^{-n}$	7.82	6.63	7.16	14.87
	1/n	0.45	0.44	0.39	0.44
	R^2	0.940	0.991	0.951	0.988

Table 4.18 Isotherm parameters of 2,4-D adsorption onto the optimum biochar

Models	Parameters	Biochar			
		CCB	RHB	BAB	CFB
Langmuir	Q_0 (mg/g)	41.7	28.6	36.7	367.7
	K_L (L/mg)	0.46	0.74	0.98	0.05
	R_L	0.0010	0.0014	0.0011	0.0001
	R^2	0.993	0.956	0.996	0.968
Freundlich	K_F (mg g^{-1}) (mg L^{-1}) $^{-n}$	14.21	12.83	17.58	18.36
	1/n	0.40	0.31	0.32	0.84
	R^2	0.922	0.998	0.926	0.953

Table 4.19 Isotherm parameters of dichlorvos adsorption onto the optimum biochars

Models	Parameters	Biochar			
		CCB	RHB	BAB	CFB
Langmuir	Q_0 (mg/g)	29.9	40.3	28.0	90.9
	K_L (L/mg)	0.32	0.18	0.16	0.09
	R_L	0.0013	0.0010	0.0014	0.0004
	R^2	0.992	0.999	0.999	0.992
Freundlich	K_F (mg g^{-1}) (mg L^{-1}) $^{-n}$	7.07	6.17	4.32	7.99
	1/n	0.66	0.71	0.67	0.84
	R^2	0.998	0.992	0.999	0.987

Table 4.20 Isotherm parameters of pymetrozine adsorption onto the optimum biochars

Models	Parameters	The pesticides			
		CCB	RHB	BAB	CFB
Langmuir	Q_0 (mg/g)	38.3	25.9	20.8	94.4
	K_L (L/mg)	0.51	0.57	1.19	0.20
	R_L	0.0010	0.0015	0.0019	0.0004
	R^2	0.997	1.000	0.978	0.995
Freundlich	K_F (mg g^{-1}) (mg L^{-1}) $^{-n}$	12.38	9.12	10.45	15.00
	1/n	0.66	0.54	0.36	0.82
	R^2	0.982	0.979	0.878	0.985

4.5.2. The shape of the isotherm models of biochar and pesticides

The shape of the isotherms of biochar and pesticides illustrates two forms including H and L shapes (Figures 53, 54, 55 and 56). Both H and L shapes of isotherms illustrates chemisorption interaction (Somasundaran, 2004). The isotherm of the CFB and four pesticides express the H shape. The H type isotherm illustrates very strong adsorption between the pesticides and biochar (Somasundaran, 2004), this is due to the high specific surface area of CFB (Table 12) led to more adsorption sites for pesticides (G. Tan et al., 2016). On the other hand, the isotherm of the CCB, RHB, and BAB and dichlorvos express the H shape of the isotherm. This is expounded by the molecular size of the pesticides (Table 22), the diameter geometry of dichlovors is smaller than those of another pesticides. This is due to the quick transfer into the pores of the biochar. The potential density of adsorption depends on the molecular diameter of the adsorbate, the smaller in the molecular diameter of the adsorbate is more advantageous to reach the maximum adsorption capacity via the pore-filling mechanism (Nguyen, Cho, Poster, & Ball, 2007).

Table 4.21 The geometry of the molecular dimension of pesticides were determined by ChemBio3D software

Pesticides	Dimension (length x width x height)
Atrazine	0.86 x 0.36 x 0.32 nm
2,4-D Na	1.54 x 0.56 x 0.22 nm
Dichlorvos	0.73 x 0.26 x 0.61 nm
Pymetrozine	1.11 x 0.19 x 0.56 nm

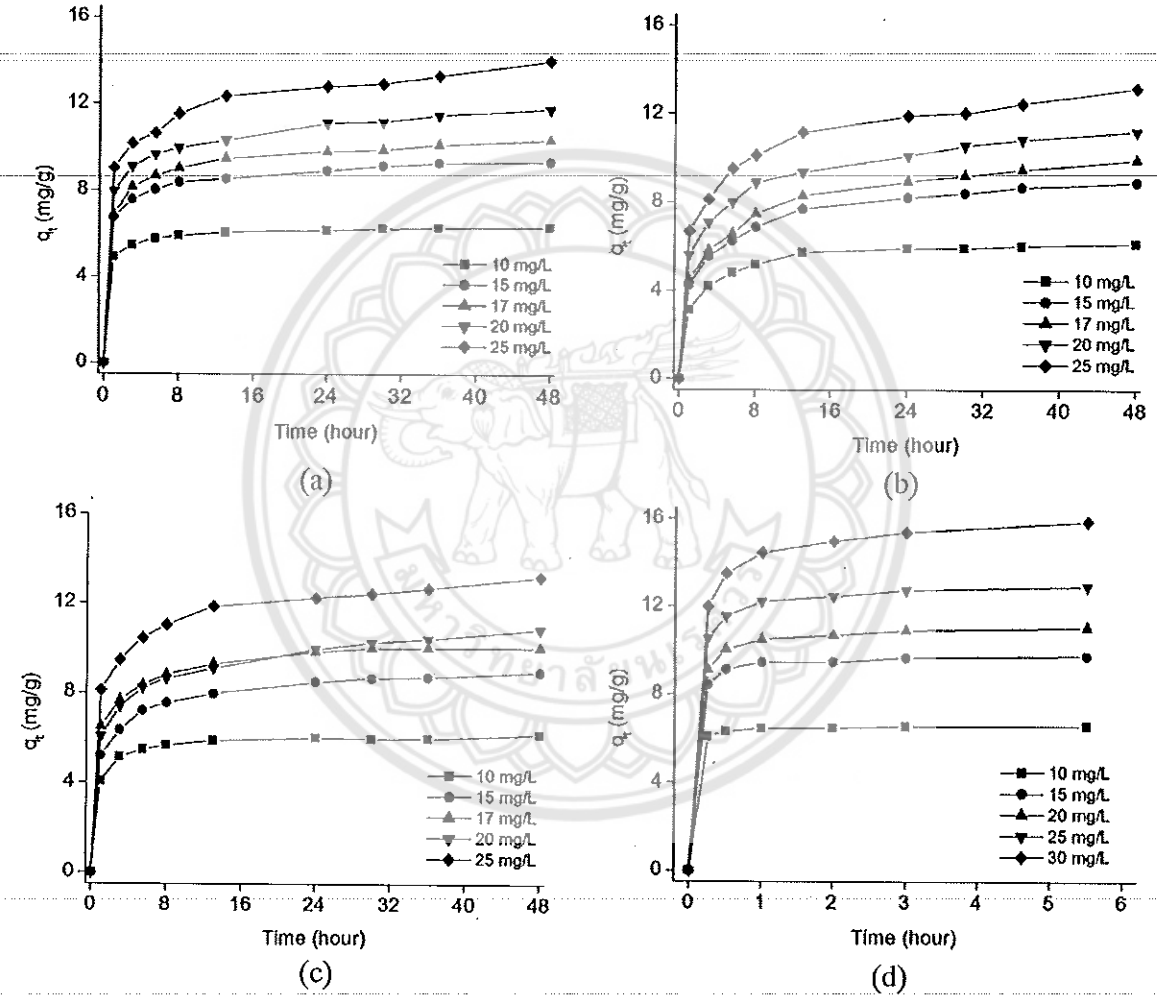

Figure 4.22 The capacities of atrazine adsorption on optimum biochars: (a) CCB, (b) RHB, (c) BAB, (d) CFB

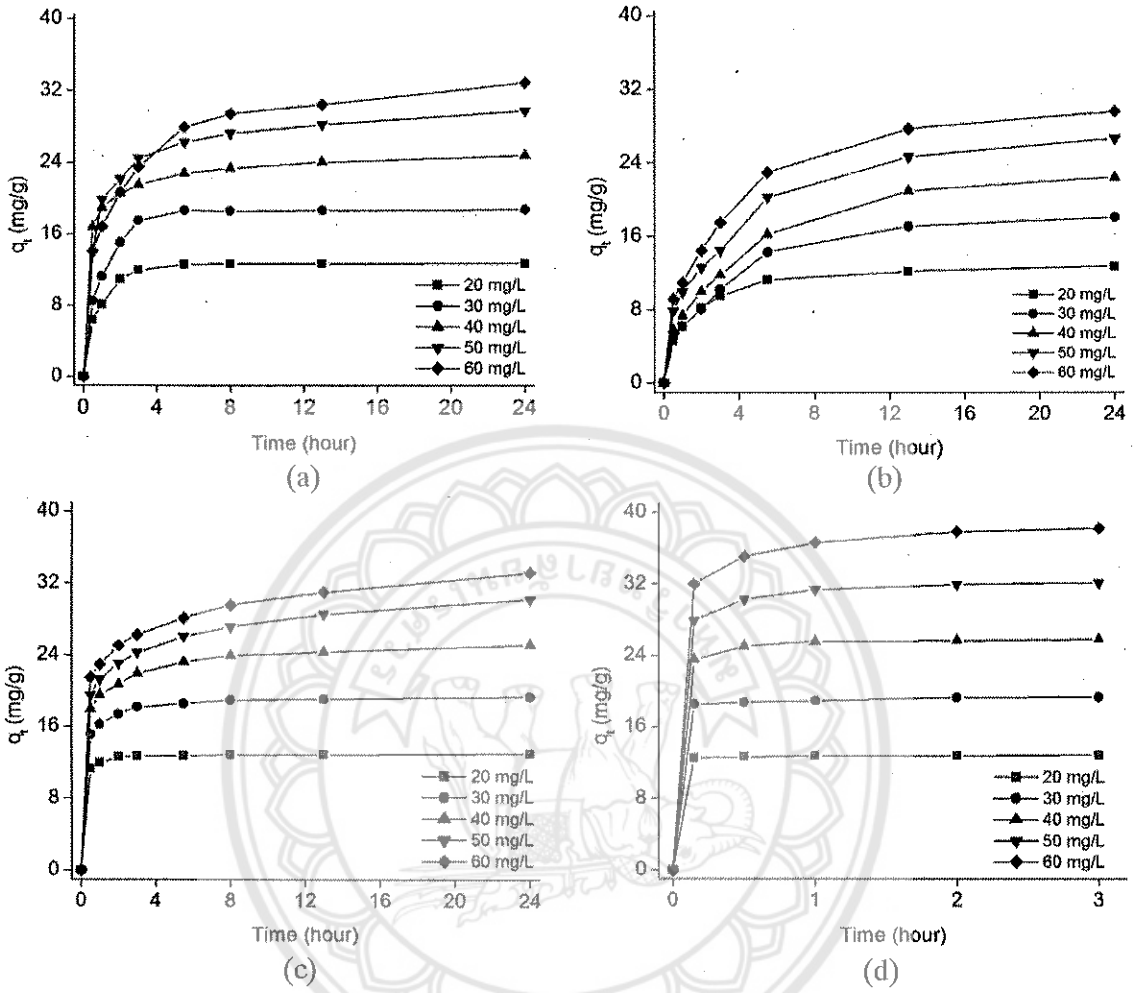

Figure 4.23 The capacities of 2,4-D adsorption on optimum biochars: (a) CCB, (b) RHB, (c) BAB, (d) CFB

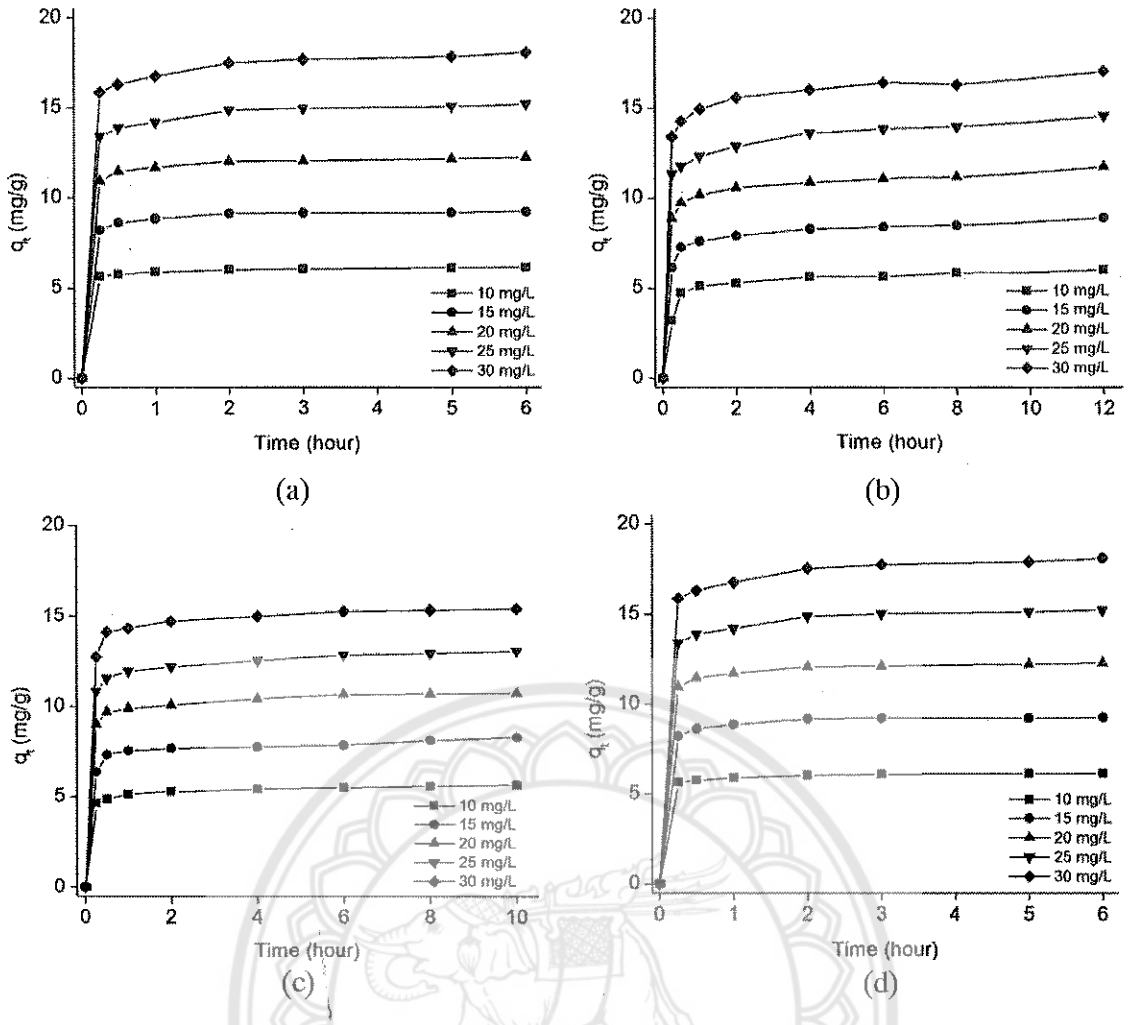

Figure 4.24 The capacities of dichlorvos adsorption on optimum biochars: (a) CCB, (b) RHB, (c) BAB, (d) CFB

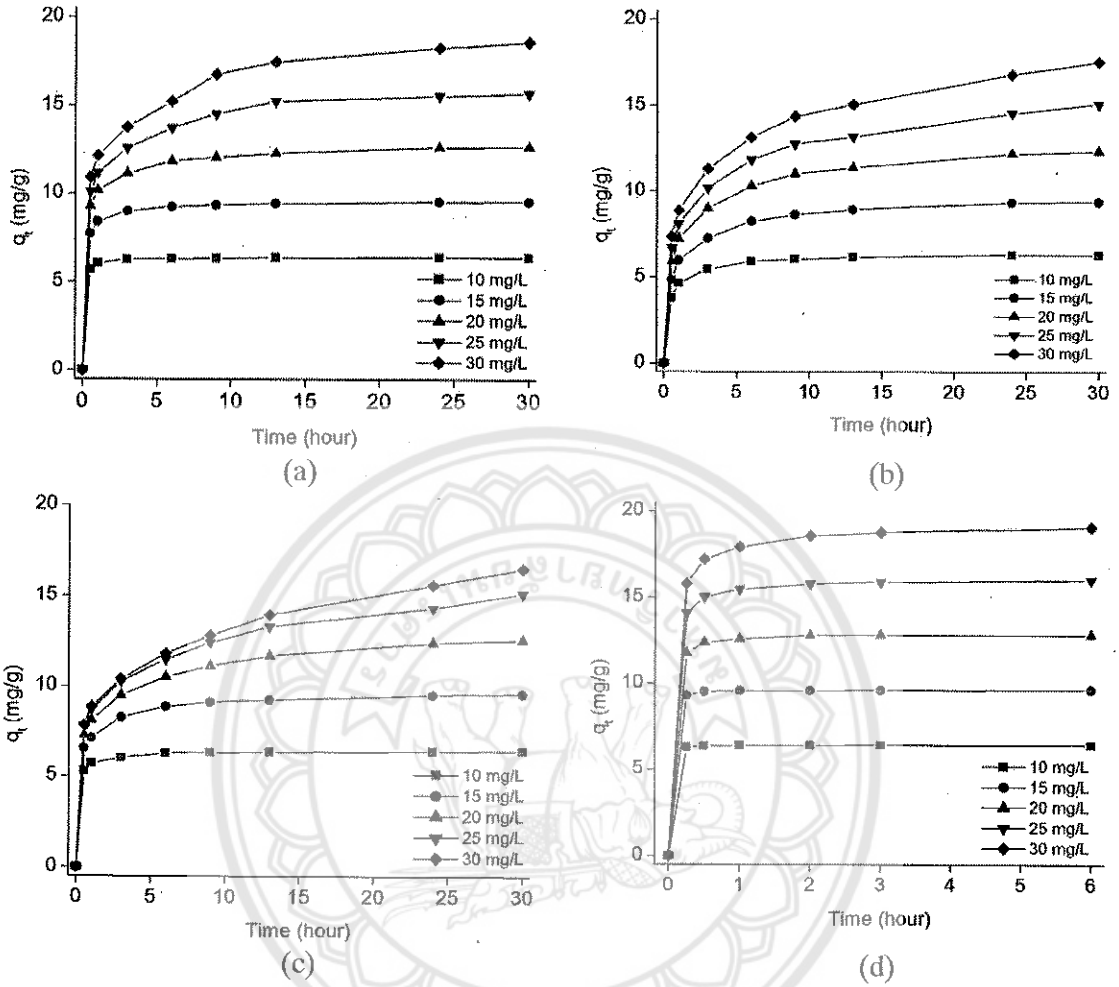

Figure 4.25 The capacities of pymetrozine adsorption on optimum biochars: (a) CCB, (b) RHB, (c) BAB, (d) CFB

Chapter 5
Conslussion

In this study, the yield of the biochar decreased significantly, when the biomass was pyrolysed at high temperatures. However, the increasing of the holding time caused the yields of the biochar to decrease a little. When the pyrolysis temperatures were increased, the Q_0 of the biochar were significantly increased. When the holding times of the pyrolysis process were increased, the Q_0 of the biochar increased slightly. However, at high pyrolysis temperatures and a long holding time, the biochar pores were destroyed, causing a decrease of the Q_0.

The four kinds of biochar were synthesised under different pyrolysis conditions and modified with HCl. They had the highest atrazine adsorption including CCB600 ^{0}C-4 h, RHB500 ^{0}C-6 h, BAB600 ^{0}C-6 h, CFB600 ^{0}C-4 h. The best of the four kinds of biochar that was modified with different acids which have a high atrazine adsorption including: CCB600 ^{0}C-4 h washing with HF (CCB), RHB500 ^{0}C-6 h washing with HF (RHB), BAB600 ^{0}C-6 h washing with HF-H_2SO_4 (BAB),
CFB600 ^{0}C-4 h washing with HCl (CFB).

The pH_{pzc} values of the four kinds of biochar CCB, RHB, BAB, and CFB were 0.7 to 0.75. The specific surface areas of the optimum biochars, i.e. CCB, RHB, BAB, and CFB were 292.92, 153.27, 67.42, 402.43 m^2/g, respectively. The four kinds of biochar present the hydrophilic properties. The optimum pH of the solution that engendered the highest removal of atrazine, 2,4-D, and pymetrozine adsorbed onto the four kinds of biochar were approximately at 1.5, 2.0, between 3 and 4.0, respectively.

The adsorption capacity depended on the specific surface area and the total pore volume of the biochar. The adsorption kinetics of the pesticides and the four kinds of biochar best fitted the pseudo-second-order model. The data of the isotherm model of the pesticides and the four kinds of biochar fitted the Langmuir isotherm. However, the adsorption data of the CCB and diclorvos, the RHB and 2,4-D, and the CFB and atrazine were best described according to the Freundlich model. The H shape isotherm of the CFB and pesticides, and the four kinds of biochar and dichlorvos
showed a very powerful adsorption capacity. The liquid film diffusion was the rate limiting step and the main diffusion mechanism of pesticides onto biochar.

The adsorption mechanisms between the four kinds of biochar and the pesticides include the pore-filling mechanism and the chemical interaction. However, the chemisorption mechanism between each of pesticides and biochar were different. The H-bonding, hydrophobic bonds, and π–π EDA are interactions in the adsorption mechanism of atrazine, pymetrozine and the four kinds of biochar. H-bonding and π-π EDA interactions participated in the adsorption mechanism of biochar and 2,4-D. For dichlorvos, H-bonding and hydrophobic bonds are chemical interactions in the adsorption mechanism. In the adsorption mechanism of the four kinds of biochar and the four types of pesticide, H-bonding interaction plays an important role and is the main chemical adsorption mechanism.

From the overall results in this study, biochar was synthesised from corn cob, rice husk, bagasse, and coconut fibre biomass which had a high efficiency of pesticide adsorption, while coconut fibre shows the strongest adsorption of pesticides. Therefore, the four kinds of biochar were effective materials and have great potential to improve the treatment of environmental pollutants.

Reference

Ahmad, A. L., Loh, M. M., & Aziz, J. A. (2007). Preparation and characterization of activated carbon from oil palm wood and its evaluation on Methylene blue adsorption. *Dyes and Pigments, 75*(2), 263-272. doi: http://dx.doi.org/10.1016/j.dyepig.2006.05.034

Australian, A. g. (2008). Dichlorvos Environmental Assessment. In A. P. a. V. M. A. 2008 (Ed.). PO Box E 240, Kingston ACT 2604, Australia.

Cerovic´, L. S., Milonjic´, S. K., Todorovic´, M. B., Trtanj, M. I., Pogozhev, Y. S., Blagoveschenskii, Y., & Levashov, E. A. (2007). Point of zero charge of different carbides. *Colloids and Surfaces A: Physicochemical and Engineering Aspects, 297*(1), 1-6. doi: https://doi.org/10.1016/j.colsurfa.2006.10.012

Chen, D., Zhou, J., & Zhang, Q. (2014). Effects of heating rate on slow pyrolysis behavior, kinetic parameters and products properties of moso bamboo. *Bioresource Technology, 169*, 313-319. doi: http://dx.doi.org/10.1016/j.biortech.2014.07.009

Chen, X., Chen, G., Chen, L., Chen, Y., Lehmann, J., McBride, M. B., & Hay, A. G. (2011). Adsorption of copper and zinc by biochars produced from pyrolysis of hardwood and corn straw in aqueous solution. *Bioresource Technology, 102*(19), 8877-8884. doi: https://doi.org/10.1016/j.biortech.2011.06.078

Chun, Y., Sheng, G., Chiou, C. T., & Xing, B. (2004). Compositions and sorptive properties of Crop Residue-Derived Chars. *Environmental Science & Technology, 38*, 4649-4655.

Damalas, C. A., & Eleftherohorinos, I. G. (2011). Pesticide exposure, safety issues, and risk assessment indicators. *International Journal of Environmental Research and Public Health, 8*(5), 1402-1419.

Degheele, D. (1998). Insecticides with novel modes of action (1 ed., pp. 289-304): Springer-Verlag Berlin Heidelberg.

Demirbar, A. (2009). Chapter 2. Fuels from biomass *Biohydrogen for future enegine Fuel Demand* (pp. 276). Springer Verlag London.

EFSA, E. F. S. A. (2014). Conclusion on the peer review of the pesticide risk assessment of the active substance pymetrozine.

Environmental, E. M. a. P. M. (1999). Environmental Fate of 2,4-Dichlorophenoxyacetic Acid (D. o. P. R. Environmental Monitoring and Pest Management, Trans.). Sacramento, CA 95814-3510.

EPA. (2006b). Reregistration Eligibility Decision for Dichlorvos. Washington D.C, USA.

EPA, E. P. A. (2000). Pymetrozine. Washington D.C, USA.

Essandoh, M., Wolgemuth, D., Jr., C. U. P., Mohan, D., & Mlsna, T. (2017). Phenoxy herbicide removal from aqueous solutions using fast pyrolysis switchgrass biochar. *Chemosphere, 174*, 49-57. doi: http://doi.org/10.1016/j.chemosphere.2017.01.105

EURL-SRM. (2016). Analysis of Pymetrozine by the QuEChERS Method. Germany.

European, E. C. H. C. P. D.-G. (2002). Pymetrozine. York, United Kingdom.

FAO and WHO, F. a. A. O. o. t. U. N., World Health Organization. (2014). Pesticide residues in food 2014.

Federal, F. I. f. R. A. (2014). Pymetrozine. Federal Institute for Risk Assessment, Berlin, Germany.

Fu, P., Hu, S., Xinag, J., Sun, L., Yang, T., Zhang, A., . . . Chen, G. (2009). Effects of Pyrolysis Temperature on Characteristics of Porosity in Biomass Chars. Paper presented at the International Conference on Energy and Environment Technology, Guilin, Guangxi, China.

Gai, X., Wang, H., Liu, J., Zhai, L., Liu, S., Ren, T., & Liu, H. (2014). Effects of Feedstock and Pyrolysis temperature on Biochar Adsorption of Ammonium and Nitrate. *Plos one, 9*(12), 1. doi: 10.1371/journal.pone.0113888

Gatabi, M. P., Moghaddam, H. M., & Ghorbani, M. (2016). Point of zero charge of maghemite decorated multiwalled carbon nanotubes fabricated by chemical precipitation method. *Journal of Molecular Liquids, 216*(Supplement C), 117-125. doi: https://doi.org/10.1016/j.molliq.2015.12.087

Ghosh, P. K., & Philip, L. (2005). Performance Evaluation of Waste Activated Carbon on Atrazine Removal from Contaminated Water. *Journal of Environmental Science and Health Part B, 40*(2005), 425-441. doi: 10.1081/PFC-200047576

Goertzen, S. L., The´riault, K. D., Oickle, A. M., Tarasuk, A. C., & Andreas, H. A. (2010). Standardization of the Boehm titration. Part I. CO2 expulsion and endpoint determination. *Carbon, 48*(4), 1252-1261. doi: https://doi.org/10.1016/j.carbon.2009.11.050

Gomez, S., Lerici, L., Saux, C., Perez, A. L., Brondino, C. D., Pierella, L., & Pizzio, L. (2017). Fe/ZSM-11 as a novel and efficient photocatalyst to degrade Dichlorvos on water solutions. *Applied Catalysis B: Environmental, 202*, 580-586. doi: https://doi.org/10.1016/j.apcatb.2016.09.047

Guo, J., & Lua, A. C. (1998). Characterization of chars pyrolyzed from oil palm stones for the preparation of activated carbons. *Journal of Analytical and Applied Pyrolysis, 46*(1998), 113–125.

Hafshejani, L. D., Hooshmand, A., Naseri, A. A., Mohammadi, A. S., Abbasi, F., & Bhatnagar, A. (2016). Removal of nitrate from aqueous solution by modified sugarcane bagasse biochar. *Ecological Engineering, 95*, 101-111. doi: http://dx.doi.org/10.1016/j.ecoleng.2016.06.035

Hai Liu, Jian Zhang, Huu Hao Ngo, Wenshan Guo, Haiming Wu, Zizhang Guo, . . . Zhang, a. C. (2015). Effect on physical and chemical characteristics of activated carbon on adsorption of trimethoprim: mechanisms study. *RSC Advances, 5*, 85187–85195. doi: 10.1039/c5ra17968h

Hattab, M. T. A., & Ghaly, A. E. (2012). Disposal and Treatment Methods for Pesticide Containing Wastewaters: Critical Review and Comparative Analysis *Journal of Environmental Protection, 3*, 431-453

Herold, A. E., Beardmore, R. A., & Parrish, S. K. (2003). USA Patent No.

IARC, I. A. f. R. o. C. (1999). Some Chemicals that Cause Tumours of the Kidney or Urinary Bladder in Rodents and Some Other Substances (Vol. 73).

Inyang, M., & Dickenson, E. (2015). The potential role of biochar in the removal of organic and microbial contaminants from potable and reuse water: A review. *Chemosphere, 134*, 232-240. doi: http://dx.doi.org/10.1016/j.chemosphere.2015.03.072

IUPAC. (2014). Compendium of Chemical Terminology Gold book (Version 2.3.3).

Kinney, T. J., Masiello, C. A., Dugan, B., Hockaday, W. C., Dean, M. R., Zygourakis, K., & Barnes, R. T. (2012). Hydrologic properties of biochars produced at different temperatures. *Biomass and Bioenergy, 41*, 34-43. doi: https://doi.org/10.1016/j.biombioe.2012.01.033

Komnitsas, K., Zaharaki, D., Bartzas, G., & Alevizos, G. (2017). Adsorption of scandium and neodymium on biochar derived after low-temperature pyrolysis of sawdust. *Minerals, 7*, 1-18.

Krzesin´ska, M., & Zachariasz, J. (2007). The effect of pyrolysis temperature on the physical properties of monolithic carbons derived from solid iron bamboo. *Journal of Analytical and Applied Pyrolysis, 80*(1), 209-215. doi: https://doi.org/10.1016/j.jaap.2007.02.009

Lakherwal, D. (2014). Adsorption of Heavy Metals: A Review *International Journal of Environmental Research and Development, 4*(1), 41-48.

Liu, H., Zhang, J., Ngo, H. H., Guo, W., Wu, H., Guo, Z., . . . Zhang, C. (2015). Effect on physical and chemical characteristics of activated carbon on adsorption of trimethoprim: mechanisms study. *RSC Advances, 5*, 85187–85195. doi: 10.1039/c5ra17968h

Liu, N., Charrua, A. B., Weng, C.-H., Yuan, X., & Ding, F. (2015). Characterization of biochars derived from agriculture wastes and their adsorptive removal of atrazine from aqueous solution: A comparative study. *Bioresource Technology, 198*, 55-62. doi: http://dx.doi.org/10.1016/j.biortech.2015.08.129

Liu, N., Zhu, M., Wang, H., & Ma, H. (2016). Adsorption characteristics of Direct Red 23 from aqueous solution by biochar. *Journal of Molecular Liquids, 223*, 335-342. doi: http://dx.doi.org/10.1016/j.molliq.2016.08.061

Liu, Z., Dugan, B., Masiello, C. A., & Gonnermann, H. M. (2017). Biochar particle size, shape, and porosity act together to influence soil water properties. *Plos one, 12*(6), 1-19.

Melo, L. C. A., Coscione, A. R., Abreu, C. A., Puga, A. P., & Camargo, O. A. (2013). Influence of pyrolysis temperature on Cadmium and Zinc sorption capacity of Sugar Cane straw – Derived biochar. *Peer-Reviewed Article, 8*(4), 4992-5004.

Mukherjee, A., Zimmerman, A. R., & Harris, W. (2011). Surface chemistry variations among a series of laboratory-produced biochars. *Geoderma, 163*(3), 247-255. doi: https://doi.org/10.1016/j.geoderma.2011.04.021

Narayanan, N., Gupta, S., Gajbhiye, V. T., & Manjaiah, K. M. (2017). Optimization of isotherm models for pesticide sorption on biopolymer-nanoclay composite by error analysis. *Chemosphere, 173*, 502-511. doi: http://dx.doi.org/10.1016/j.chemosphere.2017.01.084

Nguyen, T. H., Cho, H.-H., Poster, D. L., & Ball, W. P. (2007). Evidence for a pore-filling mechanism in the adsorption of aromatic hydrocarbons to a natural wood char. *Environmental Science & Technology, 41*(4), 1212-1217.

Njoku, V. O., & Hameed, B. H. (2011). Preparation and characterization of activated carbon from corncob by chemical activation with H3PO4 for 2,4-dichlorophenoxyacetic acid adsorption. *Chemical Engineering Journal, 173*(2), 391-399. doi: https://doi.org/10.1016/j.cej.2011.07.075

Nuithitikul, K., Srikhun, S., & Hirunpraditkoon, S. (2010). Kinetics and equilibrium adsorption of Basic Green 4 dye on activated carbon derived from durian peel: Effects of pyrolysis and post-treatment conditions. *Journal of the Taiwan Institute of Chemical Engineers, 41*(5), 591-598. doi: https://doi.org/10.1016/j.jtice.2010.01.007

Qurratu, A., & Reehan, A. (2016). A Review of 2,4-Dichlorophenoxyacetic Acid (2,4-D) Derivatives: 2,4-D Dimethylamine Salt and 2,4-D Butyl Ester. *International Journal of Applied Engineering Research, 11*(19), 9946-9955

Rahman, M. A., & Muneer, M. (2005). Photocatalysed degradation of two selected pesticide derivatives, dichlorvos and phosphamidon, in aqueous suspensions of titanium dioxide. *Desalination, 181*(1), 161-172. doi: https://doi.org/10.1016/j.desal.2005.02.019

Saffari, M., Karimian, N., Ronaghi, A., Yasrebi, J., & Ghasemi-Fasaei, R. (2015). Stabilization of nickel in a contaminated calcareous soil amended with low-cost amendments. *Journal of Soil Science and Plant Nutrition, 15*(4), 896-913.

Saleh, S., Kamarudin, K. B., Ghania, W. A. W. A. K., & Kheang, L. S. (2016). Removal of Organic Contaminant from Aqueous Solution Using Magnetic Biochar. *Procedia Engineering, 148*, 228-235. doi: http://dx.doi.org/10.1016/j.proeng.2016.06.590

Santos, L. B. O. d., & Masini, J. C. (2015). Sequential Injection Analysis with Square Wave Voltammetry (SI-SWV) Detection for Investigation of Adsorption of Picloram on a Clay Soil. *Journal of the Brazilian Chemical Society, 26*(10), 2063-2068.

Somasundaran, P. (2004). *Encyclopedia of surface and colloid Science*: CRC Press.

Sykes, P. (1985). Electrophilic and nucleophilic substitution in aromatic systems *Mechanism in organic chemistry* (Sixth edittion ed., pp. 155-156). United States with John Wiley and Sons, Inc. New York: Longman Scientific and Technical, Copublished in the United States with John Wiley and Sons, Inc. New York.

Tan, G., Sun, W., Xu, Y., Wang, H., & Xu, N. (2016). Sorption of mercury (II) and atrazine by biochar, modified biochars and biochar based activated carbon in aqueous solution. *Bioresource Technology, 211*, 727-735. doi: http://dx.doi.org/10.1016/j.biortech.2016.03.147

Tan, X., Liu, Y., Zeng, G., Wang, X., Hu, X., Gu, Y., & Yang, Z. (2015). Application of biochar for the removal of pollutants from aqueous solutions. *Chemosphere, 125*, 70-85. doi: http://doi.org/10.1016/j.chemosphere.2014.12.058

Tran, H. N., Wang, Y.-F., You, S.-J., & Chao, H.-P. (2017). Insights into the mechanism of cationic dye adsorption on activated charcoal: The importance of π–π interactions. *Process Safety and Environmental Protection, 107*(Supplement C), 168-180. doi: https://doi.org/10.1016/j.psep.2017.02.010

Trivedi, N. S., Kharkar, R. A., & Mandavgane, S. A. (2016). Utilization of cotton plant ash and char for removal of 2, 4-dichlorophenoxyacetic acid. *Resource-Efficient Technologies, 2, Supplement 1*, S39-S46. doi: http://doi.org/10.1016/j.reffit.2016.11.001

Uchimiya, M., Wartelle, L. H., & Boddu, V. M. (2012). Sorption of Triazine and Organophosphorus Pesticides on Soil and Biochar. *Agricultural and food chemistry, 60*, 2989–2997.

Varsha Srivastava, C. H. Weng, V. K. Singh, & Sharma, a. Y. C. (2011). Adsorption of Nickel Ions from Aqueous Solutions by Nano Alumina: Kinetic, Mass Transfer, and Equilibrium Studies. *Chemical and engineering data, 56*, 1414-1422.

Wang, L., Yan, W., He, C., Wen, H., Cai, Z., Wang, Z., . . . Liu, W. (2018). Microwave-assisted preparation of nitrogen-doped biochars by ammonium acetate activation for adsorption of acid red 18. *Applied Surface Science, 433*, 222-231. doi: https://doi.org/10.1016/j.apsusc.2017.10.031

WHO. (2003). 2,4-D in Drinking-water.

Atrazine and Its Metabolites in Drinking-water (2011).

WHO, I. (1999). IARC monographs on the evaluation of carcinogenic risks to humans, Some chemicals that cause tumours of the kidney or urinary bladder in rodents and some other substances (Vol. 73, pp. 59-113). Lyon, France.

WHO, W. H. O. (2007). Dichlorvos in Drinking-water.

Yakout, S. M., Daifullah, A. E. H. M., & El-Reefy, S. A. (2015). Pore structure characterization of chemically modified biochar derived from rice straw. *Environmental Engineering and Management Journal, 14*(2), 473-480.

Yavari, S., Malakahmad, A., & Sapari, N. B. (2015). Biochar efficiency in pesticides sorption as a function of production variables—a review. *Environmental Science and Pollution Research, 22*(18), 13824-13841.

Yue, L., Ge, C., Feng, D., Yu, H., Deng, H., & Fu, B. (2017). Adsorption–desorption behavior of atrazine on agricultural soils in China. *Journal of Environmental Sciences, 57*, 180-189. doi: https://doi.org/10.1016/j.jes.2016.11.002

Zhang, Y., Liu, G., Chen, L., & Zheng, H. (2016). *Adsorption of chlorpyrifos on giant reed derived biochars* Paper presented at the International Conference on Civil, Transportation and Environment (ICCTE 2016)